Applied Materials Today 14 (2019) 1–20

Contents lists available at ScienceDirect

Applied Materials Today

journal homepage: www.elsevier.com/locate/apmt

One-dimensional anodic TiO_2 nanotubes coated by atomic layer deposition: Towards advanced applications

Filip Dvorak[a], Raul Zazpe[a,b], Milos Krbal[a], Hanna Sopha[a,b], Jan Prikryl[a], Siowwoon Ng[b], Ludek Hromadko[a], Filip Bures[c], Jan M. Macak[a,b,*]

[a] Center of Materials and Nanotechnologies, Faculty of Chemical Technology, University of Pardubice, Nam. Cs. Legii 565, 53002 Pardubice, Czech Republic
[b] Central European Institute of Technology, Brno University of Technology, Purkynova 123, 612 00 Brno, Czech Republic
[c] Institute of Organic Chemistry and Technology, Faculty of Chemical Technology, University of Pardubice, Studentska 573, 53210 Pardubice, Czech Republic

ARTICLE INFO

Article history:
Received 21 September 2018
Received in revised form 11 October 2018
Accepted 2 November 2018

Keywords:
Atomic layer deposition
TiO_2 nanotube
Coatings
Functionalization
Aspect ratio

ABSTRACT

Atomic layer deposition (ALD) represents a unique deposition technique that allows to coat uniformly various high aspect ratio (HAR) porous nanostructures, in addition to its traditional role to coat flat substrates (e.g. Si wafers). Self-organized anodic TiO_2 nanotube (TNT) layers belong among the most investigated inorganic nanostructures. They possess highly functional materials with promising application potential across many technological fields. Herein, we review the utilization of ALD for the functionalization of anodic TNT layers by secondary materials to advance their physicochemical and photoelectrochemical properties. First, the application of ALD for functionalization of porous aluminium oxide, which represent fundamental HAR nanostructure, is briefly introduced. Then the main experimental parameters governing the uniformity and the conformality of ALD coating within HAR nanostructures are discussed. Finally, the review focuses on the use of ALD to deposit secondary materials into TNT layers for various purposes — the introduction of pioneering studies is followed by particular examples of ALD based functionalizations of coated TNT layers for optimized visible-light absorption, charge separation and passivation, (photo)catalysis, stability, gas sensing, and energy storage.

Contents

Abbreviations: AAO, anodic aluminium oxide; ALD, atomic layer deposition; CBD, chemical bath deposition; DSSC, dye-sensitized solar cell; EDX, energy-dispersive X-ray spectroscopy; EOR, ethanol oxidation reaction; FTIR, Fourier transform infrared spectroscopy; HAADF, high-angle annular dark-field; (H)AR, (high) aspect ratio; IPCE, incident photon to electron conversion efficiency; MB, methylene blue; MC, Monte Carlo; PEC, photoelectrochemical; QCM, quartz crystal microbalance; QD, quantum dots; SEM, scanning electron microscope; SILAR, successive ionic layer adsorption and reaction; (S)TEM, (scanning) transmission electron microscope; TMA, trimethylaluminium; TNT, TiO_2 nanotube; UV, ultraviolet spectral range; vis, visible spectral range; XRR, X-ray reflectivity.

* Corresponding author.
E-mail address: jan.macak@upce.cz (J.M. Macak).

https://doi.org/10.1016/j.apmt.2018.11.005

1. Introduction

Titanium dioxide (TiO_2) represents a fascinating and highly functional material. Until now, TiO_2 has found its main commercial applications in pigments, food industry and cosmetics. Pioneering observation of photocatalytic decomposition of water at TiO_2 electrode in 1970s [1] launched the tremendous interest in the development of applications of TiO_2 in solar energy conversion, energy storage, and photo-assisted bioremediation, which represent essential components for the concept of renewable energy sources and of sustainable environment [2]. These applications also take the advantages of TiO_2 to be a low cost material with an extremely low photocorrosion rate. Additionally, thanks to inherent biocompatibility, low toxicity, and high chemical stability of TiO_2, emergence of biomedical applications of TiO_2, including photodynamic therapy for cancer treatment, drug delivery systems, cell imaging, biosensors, and genetic engineering has also taken place [3].

TiO_2 is a wide band gap (3.0–3.2 eV) n-type semiconductor and thus it absorbs light only in the UV spectral range. Generally, the material properties can be tuned by nanostructuring, realized by a gradual decrease of the characteristic size of applied materials down to the nanometer scale [4]. Nanostructuring of materials results in an extremely increased surface to volume ratio with significant impact on material physicochemical properties, including light absorption. Since many applications of TiO_2 are to great extent influenced by the surface of TiO_2 [5], nanostructuring of TiO_2 represent an important step for its efficient and flexible utilization in various applications.

Probably the most prominent utilization of nanostructured TiO_2 is represented by the utilization of TiO_2 nanoparticles in the dye-sensitized solar cell (DSSC), introduced by O'Regan and Grätzel [6] and by the recent utilization in perovskite solar cells [7,8]. Another class of nanostructured TiO_2 is presented by 1-D nanostructured materials such as nanowires, nanorods, nanobelts, and nanotubes [9]. 1-D nanomaterials share with nanoparticles (0-D materials) the high surface area and promotional size quantum confinement effects, but have one dimensions outside the nanoscale, typically pore depth or length (applies for tube, rods, wires, fibres). 1-D nanomaterials offer better unidirectional charge/reactant/ion transport properties and better mechanical integrity. TiO_2 nanotube (TNT) layers prepared by anodization of Ti represent a very popular type of 1-D material with the key advantages of facile growth, self-ordering, well-controlled geometry, scalability, high surface area, direct contact to metal-support, and suitability for coating by secondary materials [10–12]. The important characteristic parameter of TNT layers is their aspect ratio (AR), which is the ratio between length and diameter of TNT. In general, the higher AR offers the larger surface area which enhances the benefits of the nanotube structures. Another important aspect of TNT layers is their structural variability – they are amorphous in the as-anodized state, but can be converted, depending on the temperature, into anatase, rutile or their mixtures [11] with large flexibility towards applications. Last, but not least, they possess very good adhesion to the underlying Ti substrates, however, upon specific treatments, they can be detached into free-standing membranes [13,14] or nanotube powders [15].

To address complex functionalities of TNT layers in applications, it is beneficial to combine them with secondary materials. In order to keep advantages of the high surface nanotubular geometry, it is necessary to coat the entire surface of nanotubes. The most often used approaches to fill/coat the nanotube layers, such as electrodeposition [16–19], chemical bath deposition [20–22], spincoating [23,24], or sputtering [25–27], are able to uniformly coat TNTs layers with specific dimensions (predominantly with a low AR). The atomic layer deposition (ALD) represents the only deposition technique able to coat uniformly highly porous nanostructures of virtually any size [28].

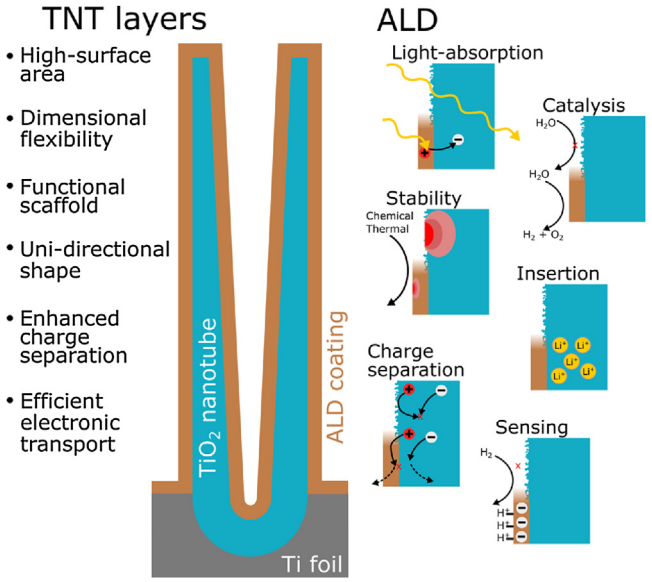

Fig. 1. Illustration of utilization of ALD for advanced functionalization of TNT layers.

ALD is an established deposition technique based on sequential self-limited adsorption of vapours of compatible precursors on surfaces leading to the formation of required coatings. The self-limited adsorption is the key aspect of ALD making it different from other deposition techniques. Under optimized conditions (temperature, pressure, and exposition time), the precursor molecules are adsorbed all over the surface in just one monolayer – further adsorption of precursor molecules on the already occupied surface sites is not allowed. No matter of the geometry of the substrate, the coatings prepared by ALD have unprecedented conformity all over the surface and their thickness is controllable on the atomic level [29]. As illustrated in Fig. 1, ALD coatings can help to tune/enhance many properties of TNT layers, such as light absorption, separation of photogenerated electron-hole pairs, photocatalytic and electrocatalytic properties, chemical, thermal, and mechanical stability, gas sensing, and energy storage. In particular, ALD is suitable for very thin coatings while it is only to a limited extent (from the point of both high precursor costs and high time demands) usable for the growth of thick coatings (>tens of nanometers). The restricted temperature window for self-limited regime of ALD deposition and high investment costs of the tools/precursors represent main drawback of nowadays ALDs, but these are overcome step by step by continuous advancements in the ALD technology and also market competition.

Recently, the usability of ALD for functional coatings of nanostructures towards energy/light-driven applications has been thoroughly reviewed [29–40]. In this review, we address the utilization of ALD to tailor the functionality of anodic TNT layers for improved performance to realize new types of devices for various purposes. First, we briefly summarize the existing literature on ALD deposition into model 1-D material – porous anodic aluminium oxide (AAO) – and introduce specific theoretical features of ALD coating of HAR (HAR) nanostructures; next we focus on the utilization of ALD for functionalization of anodic TNT layers. We introduce pioneering studies of ALD into anodic TNT layers and finally we follow by the description of the utilization of ALD for improved light absorption, charge separation, (photo)catalytic properties, stability (mechanical, thermal, and chemical), gas sensing, and energy storage of ALD modified TNT layers.

2. ALD into porous aluminium oxide — overview

Pioneering studies of utilization of ALD for functional coating of 1-D HAR nanostructures by secondary materials were performed on porous anodic aluminium oxide (AAO) – a well-established self-ordered 1-D material [41,42]. Porous AAO is characterized by its mechanical, chemical, and thermal stability, nanoscale pore diameters, high surface-area ratio and low cost fabrication. These properties attracted a considerable interest for a wide number of applications in catalysis, molecular separation, electronics and photonics, (bio)sensors, energy storage and conversion, drug delivery, and templated synthesis among others reviewed by Md Jani et al. [43].

Porous AAO can be fabricated via electrochemical anodization of aluminium. The application of appropriated processing parameters during the anodization (e.g. applied voltage, electrolyte concentration, etc.) allows a very good control of the pore size, the inter-pore distance, the thickness of the porous layer and the overall AR of the pores. The inherent high surface area and AR makes porous AAO a particularly appealing nanoscale template for investigations of the kinetics and mechanisms of the surface chemical reactions that the atomic layer deposition (ALD) method is based on. In particular, Fourier transform infrared spectroscopy (FTIR) was employed to study the binary chemical reactions to deposit SiO_2 and Al_2O_3 using porous AAO as a support [44–47]. ALD properties as sub-nanometer thickness control and uniformity of the deposited material into the pores were exploited in turn, to shrink the pore diameter of porous AAO. The reduction of the pore diameter to molecular dimensions by the deposition of Al_2O_3, TiO_2 and SiO_2 dramatically improved the gas separation properties of the porous AAO [48,49]. Elam et al. used ultrahigh AR (AR ≈ 5000) porous AAO for a comprehensive study on uniformity of ALD coating of HAR structures [50], which will be discussed in detail in the next section. ALD enables to deposit a whole range of materials into AAO as demonstrated extensively in literature. Johansson et al. first performed and demonstrated ALD of a metallic compound via the deposition of copper nanoparticles into porous AAO. Therein, homogeneous particle size and particle distribution along the pores were demonstrated [51]. Following works reported on the deposition of different metals into porous AAO using ALD, such as Pd [52], Ni and Co [53,54], Ru [55], Pt/Ir [56], Ag [57], and Pt [58]. Also, the deposition of sulfides [59], nitrides [60], a wide number of different oxides as Al_2O_3 [61–63], TiO_2 [57,62–68], Ta_2O_5 [66], Fe_2O_3 [53,54,63,69], SiO_2 [63,70–73], ZnO [63,74–78], SnO_2 [79], Co_3O_4 [80], together with heterojunctions TiO_2/Sb_2S_3/CuSCN(not ALD) [81] and NiO/Sb_2S_3 [82], multilayered structures as $SiO_2/Fe_2O_3/SiO_2$ [83,84], $Fe_3O_4/ZrO_2/Fe_3O_4$ [85], and Au−$Co_xFe_{3-x}O_4$ core–shell nanowires [86] have been reported. The successful utilization of ALD for build-up of functional nanostructures on AAO templates for tunable magnetism [69] and photovoltaic devices [81] is illustrated in Fig. 2.

Porous AAO has served as an excellent substrate to evaluate the ability of novel precursors to coat/infiltrate HAR substrates [59,70,79,80]. The ALD sub-nanometer thickness control allowed fine-tuning of pore diameters [61–63,71,72] and evaluate the impact of reduced pore diameter on the single-molecule sensing properties [61], the membrane separation properties [63,71], and the ionic transport through the nanoporous membranes [72]. The deposition of secondary materials enabled the functionalization of porous AAO as different sensors [52,56,58,68], anode for Li ion batteries [67] and photoanode for dye-sensitized solar cells [74,81,82]. Except these applications, taking the unique ALD properties of conformal deposition and the wide range of materials that can be deposited, porous AAO has been intensively exploited as a template for the synthesis of different nanostructures. Nanotubular structures of different nature were reported, such as TiN nanotubes

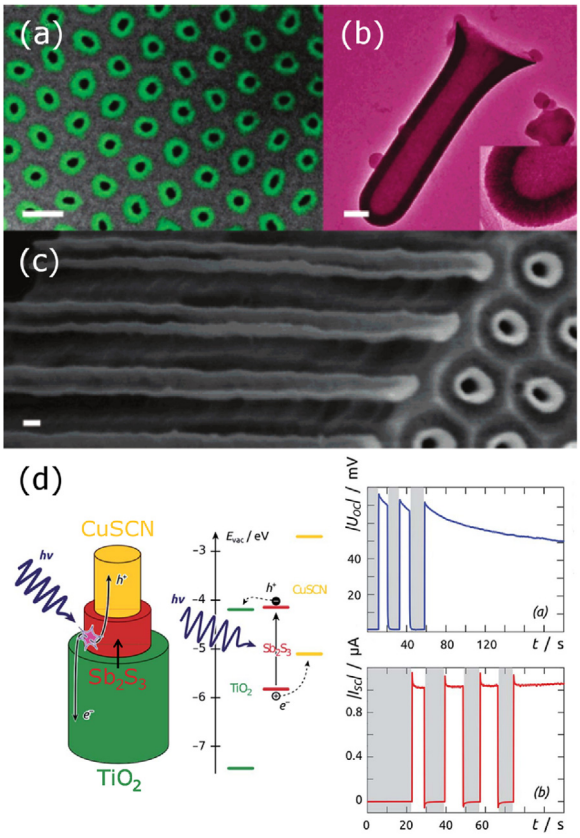

Fig. 2. Illustration of functional nanostructures based on templates of porous AAO utilizing ALD. (a)–(c) Micrographs (SEM and TEM) of ALD deposited iron oxide nanotubes for tunable magnetic properties, adopted from [69]. (d) ALD deposited TiO_2 (green) and Sb_2S_3 (red) with (not ALD) CuSCN (yellow) in AAO for integration into photovoltaic device, reproduced from [81]. (For interpretation of the references to colour in this figure legend, the reader is referred to the web version of this article.)

(exhibiting good ductility [60]), ZnO nanotubes (with superior photoluminescence characteristics [76]), or ferromagnetic nanotubes composed of Ni and Co [53,54] and Fe_2O_3 [53,54,69] shown in Fig. 2a. Single wall TNTs [64,66] and Ag loaded TiO_2 nanotubes [57], wherein an enhanced photocatalytic activity compared to unloaded TNTs was revealed, and hierarchical multiwall TNTs, fabricated via deposition of alternating TiO_2/Al_2O_3 nanolaminates followed by wet etching of sacrificial Al_2O_3 layer [65], have been also reported. The ALD benefits were also applied for the fabrication of multilayered nanotubes, such as TiO_2/Sb_2S_3/CuSCN for application in solid state solar cells [81] illustrated in Fig. 2d, and $SiO_2/Fe_2O_3/SiO_2$ [83,84] or $Fe_3O_4/ZrO_2/Fe_3O_4$ [85], whose magnetic properties were explored and their potential applications foreseen. Porous AAO also assisted the fabrication of Ru nanowire arrays as a platform for sensor devices [55] and ZnO nanorods [75,76], and ALD coated porous AAO followed by electrodeposition enabled the fabrication of complex nanostructures as TiO_2-coated Ni nanowire arrays [64], Ta_2O_5-coated Ni nanorods [66], and Au–Co ferrite nanowires [86]. Likewise, porous AAO has been proposed as suitable platform for different health and environmental applications – see Ref. [87] and references therein. In particular, ALD ZnO coated porous AAO exhibited encouraging antimicrobial activity with potential dermatological applications [77,78].

The utilization of ALD for coating porous AAO has provided a very strong motivation case for all other high-aspect 1-D nanostructures, including nanopores [88], nanotubes [89,90], nanorods [91], nanowires [92], and branching nanostructures [93,94] of various materials, to be processed in a similar fashion. Among those, TNT layers formed by anodization maintain forefront position and

promise to be treated by ALD, due to facile preparation and high functionality of TiO_2 compared to other materials.

3. Aspects of ALD into high aspect ratio nanostructures

In order to design an ALD process, leading to conformal coatings of HAR nanostructures, it is necessary to understand the kinetics and chemistry of that particular ALD process on the fundamental level. Numerous theoretical studies were devoted to the description of ALD surface chemistry and kinetics. A comprehensive review on theoretical aspects of ALD is beyond the scope of this review. Instead, in this section we want to focus on important theoretical aspects governing ALD in HAR nanostructures. The description of the ALD process in the HAR nanostructures was theoretically addressed by numerous models: a simple kinetic model [95], a kinetic model coupled with Langmuir adsorption [96], Monte Carlo (MC) based simulations in molecular [50,97–102], Knudsen and diffusive [103] gas flow regimes, and numeric or analytic solutions of Boltzmann transport equation coupled with Langmuir adsorption models [104–108]. Although the studies used different theoretical frameworks, the common idea describing the parameters leading to the conformal coating of HAR nanostructures allows to draw general qualitative overview, as follows.

One of the key aspects for achieving conformal and uniform coatings is to reach the saturation regime of on ALD deposition. This situation occurs when the precursor molecules fill (chemisorb on) all available adsorption positions of the substrate surface within every ALD cycle (leading to the saturation coverage). The corresponding saturating exposure dose (multiplication of saturation exposure time and pressure of precursor molecules) depends on the surface area (number of available adsorption positions [109]), the surface reaction probability (surface sticking coefficient), the diffusion rate, and the recombination loss probability (in case of plasma ALD processes) of precursor molecules. Fig. 3 illustrates the evolution of step coverage profiles of HAR nanostructure under characteristic deposition regimes of ALD discussed below. The light blue area together with arrows indicate the evolution of step coverage profile of HAR nanostructure (black area). Black dashed lines represent complete coverage profile under saturated regime of ALD.

Depending on the surface reaction probability of precursors and the aspect ratio (AR) of nanostructure, the formation of saturated coverage during ALD deposition into HAR structures can be limited either by the diffusion or the reaction ability of precursors [50]. The so-called reaction-limited regime takes place for low surface reaction probability of precursor molecules as compared to the diffusion probability for a given AR. This corresponds to the situation when the exposure time and pressure in combination with the sufficient diffusion rate allow precursor molecules to reach every adsorption position available within the pore/trench and the only parameter governing the coverage is the surface reaction probability. The saturating exposure dose is not affected by the porous nature of substrate to be coated and nearly equals to the saturating dose for planar surfaces with the equivalent surface area [100]. The corresponding step coverage profile of the pore/trench evolves almost uniformly with increasing exposure as it is schematically illustrated in Fig. 3a. Even unsaturated coverage within one cycle of ALD can lead to the growth of uniform coatings of HAR nanostructures. This is similar to chemical vapor deposition where the conformality increases for low reaction probabilities as a result of reduced depletion of precursors along the via [110].

On the other hand, the diffusion-limited regime occurs when the reaction probability (sticking coefficient) of precursor molecules is much larger than their diffusion probability to reach bottom of an HAR nanostructure. The precursor molecules chemisorb on the available surface sites successively from the entrance-opening of the nanostructure and the precursor coverage profile evolves in the front-like manner with the increasing exposure as depicted in Fig. 3b. The saturating exposure dose approximately scales with second power of AR [50,95]. The gradient of the coverage profile within the front is step-like for reaction probability of 100% and it gradually smoothens with decreasing reaction probability [97].

In the case of plasma ALD processes, the saturation exposure dose is strongly affected by the recombination probability of the precursors, e.g. the wall recombination of plasma radicals or ozone [100,101]. Precursor molecules rather tend to undergo recombination then to reach bottom of HAR. The coverage profiles in recombination-limited regimes are complex and not uniform, as it is drawn in Fig. 3c, and the formation of saturation coverage is possible only for the limited AR with significant saturation doses [100,106,111,112].

Repeated ALD cycles (with constant exposure time) lead to the growth of thicker coating and consequently to change of characteristic dimension/radius of opening of HAR nanostructure. As a consequence, when the thickness of coating is comparable to radius of the opening of pore), the resulting thickness profile is affected as the diffusion becomes more limited. For such cases, the exposure time throughout repeated ALD cycles needs to be properly scaled in order to achieve the uniform thickness of the final coating [107].

Generally, the works introduced above show examples of set of experimental parameters governing the uniformity of ALD coating within HAR nanostructures. The determination of the sufficient saturation dose of precursor within one ALD cycle is critical for the successful ALD of uniform coatings of HAR nanostructures. In the reality, the ALD process is influenced by many experimental parameters depending on type of precursor, substrate material, ALD process parameters, and/or ALD reactor design. The results of simulation models of ALD deposition represent qualitative support for experimental determination of parameters leading to saturated regime of ALD depositions, which need to be performed and optimized for each system and coating material individually.

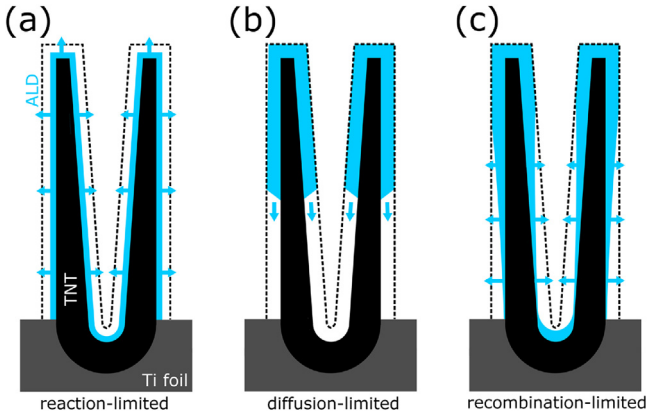

Fig. 3. The illustration of evolution of step coverage profiles (light blue) of HAR nanostructure (black) by ALD under various process regimes. Light blue area and arrows indicate evolution of step coverage with increasing ALD exposure dose. Dashed black lines represent coverage profiles under saturated regime conditions (saturation exposure dose). (a) The reaction-limited, (b) the diffusion-limited, and (c) the recombination-limited regimes of ALD deposition. (For interpretation of the references to colour in this figure legend, the reader is referred to the web version of this article.)

4. ALD into TiO_2 nanotube layers

Anodic TiO_2 nanotubes, prepared by the anodization of Ti, got into the forefront of 1-D nanostructured inorganic materials

since the development of organic based electrolytes (such as ethylene glycol or glycerol), which allowed growth of HAR TNT layers [10,113,114]. The ability to prepare HAR TNT layers represents a key step for successful applications of TNT layers. The next important step in the development of TNT-based applications is their tailoring by secondary materials, which represents a target inherently suitable for ALD utilization.

4.1. Pioneering efforts

The first works devoted to coating of anodized TNT layers by ALD have been focused on sensitization of TNT layers by In_2S_3 for solar energy conversion [115] and on the role of Al_2O_3, Ta_2O_5, and TiO_2 ALD coatings on electric properties of coated TNT layers [116].

The work of Sarkar et al. [111] presents an extensive experimental study of ALD growth of In_2S_3 applied practically on the coating of TNT layers with AR of ≈62. The ALD has been performed by utilization of indium(III) acetylacetonate ($In(acac)_3$) and H_2S precursors. The authors performed thorough analysis of In_2S_3 ALD process on flat substrates first. Quartz crystal microbalance (QCM), X-ray reflectivity (XRR), and FTIR were used in order to monitor mass gains during each reactant cycles, to measure the growth per cycle and its temperature dependence, to verify the self-limited surface chemistry of utilized precursors, and to identify surface species formed during sequential surface reactions. The verified ALD process parameters with increased exposure times were utilized for sensitization of HAR TNT layers by 5 nm thick In_2S_3 ALD coating (Fig. 4a). Unfortunately, detailed SEM or TEM investigations to prove the uniformity of ALD coating of TNT layer were missing in that paper. The prominent effect of the In_2S_3 coating on the photoelectrochemical (PEC) properties of the TNT layers is illustrated in Fig. 4b. The In_2S_3 coated TNT layers exhibited a reduced optical band gap of 2.07 eV and reached 10% external quantum efficiency for photon energy >2.5 eV while the uncoated TNT layer was generally photo-inactive for photon energy <3.0 eV. The observed quantum efficiency was significantly below the theoretically predicted maximum quantum efficiency (≈70%). The limited quantum efficiency was attributed to recombination losses and charge collection/injections processes.

The work of Tupala et al. [116] presents ALD coatings of TNT layers with AR of ≈10 by selected metal oxides: Al_2O_3, Ta_2O_5, and TiO_2. TNT layers were prepared by anodization of Ti thin layers evaporated on ITO conductive glass. The TNT layers prepared on transparent conductive support are a very suitable material for solar energy applications (e.g. perovskite solar cells [8]) and their functionalization is an important technological step. The ALD was performed with established precursors: trimethylaluminium (TMA, $Al(CH_3)_3$), tantalum pentoxide ($Ta(OEt)_5$), and titanium tetraisopropoxide ($Ti(OiPr)_4$) in combination with water. The target thickness of the coating was 5 nm. The example of TiO_2 coated TNT layers is shown in Fig. 4c. TNT layers coated by ALD were shown to have higher electric conductivities (across the layer) compared to their uncoated counterparts, as shown in Fig. 4d.

Despite both these pioneering works clearly demonstrated the functionality of ALD coated TNT layers, they did not provide any direct evidence of uniformity of ALD coatings within the TNT layers (such as SEM and TEM images). The follow up work of Macak et al. [117] presented interestingly improved light trapping properties of plasma ALD In_2O_3 coated TNT layers with AR up to ≈80 together with microscopic evidence of the presence of the In_2O_3 coating. The ALD deposited In_2O_3 was found to successfully coat the entire TNT interiors with gradually decreasing thickness of the coating from 30 to 5 nm from top to the bottom of the TNT layer (with AR ≈ 80, and layer thickness of ≈8 μm), respectively. The observed thickness gradient of In_2O_3 resulted from a limitation of plasma assisted ALD

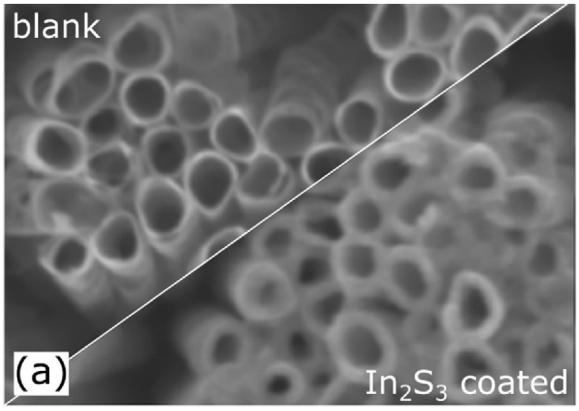

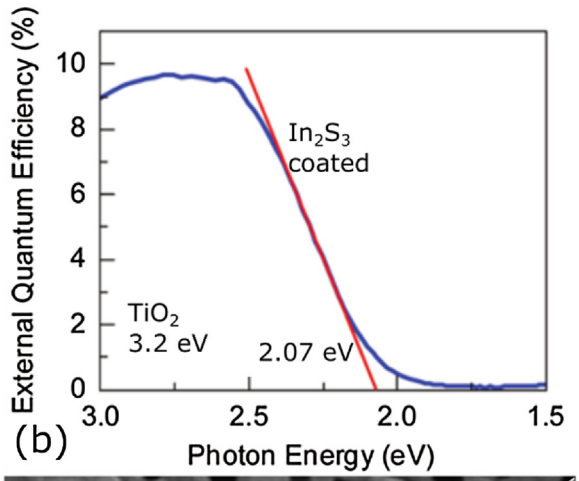

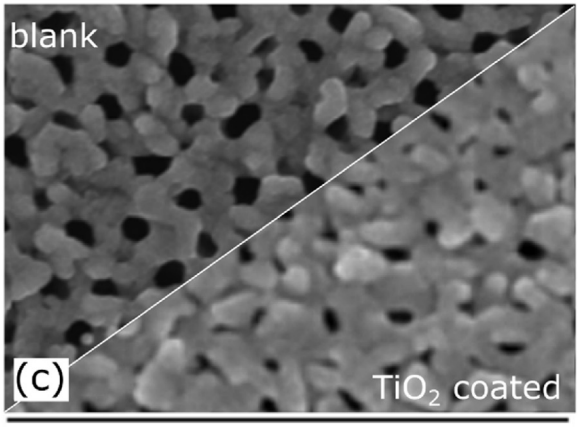

Sample	Current density at +1 V (mA cm^{-2})
Uncoated	0.9–2.5
5 nm Al_2O_3	0.12–1.28
5 nm Ta_2O_5	0.4–3.0
5 nm TiO_2	4–500

(d)

Fig. 4. Pioneering ALD coatings of TNT layers. (a) The In_2S_3 coating of TNT layers and (b) corresponding quantum efficiency. (c) The TiO_2 coated TNT layer and (d) the current density through the TNT layer modified by various metal oxide coatings. (a) and (b) were reproduced from [115] and (c) and (d) were reproduced from [116].

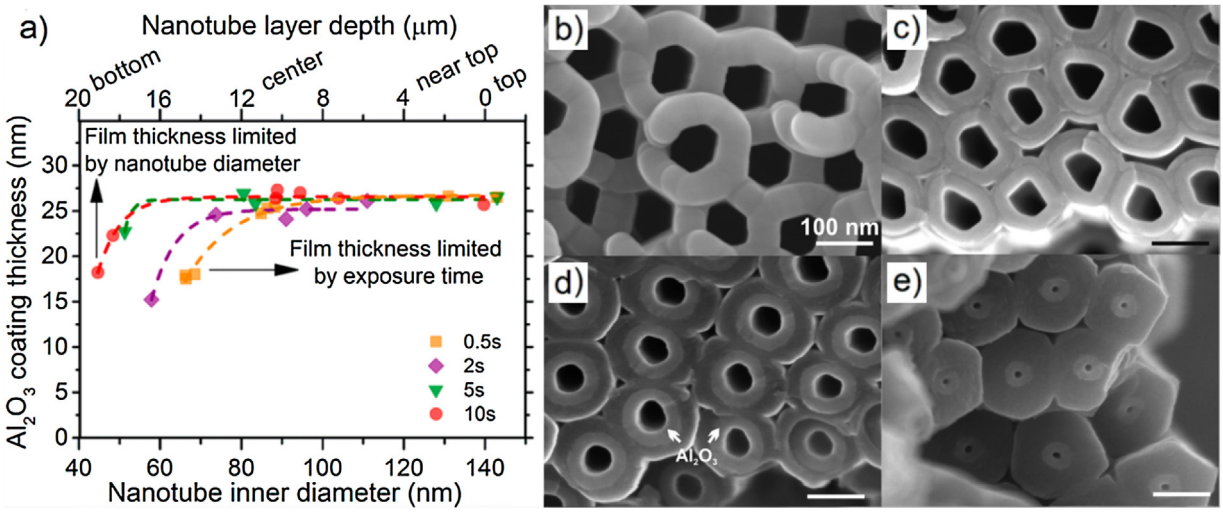

Fig. 5. ALD Al_2O_3 coating of TNT layers with aspect ratio of 180: (a) Influence of exposure time of TMA precursor during one ALD cycle on uniformity of thickness of Al_2O_3 coating within TNT layer; (b–e) Illustration of uniform thickness of Al_2O_3 coating for 5 s TMA exposure time as revealed by SEM inspection through four different depth levels – top, near-top, middle, and bottom, respectively. Reproduced from [118].

to coat uniformly HAR nanostructures due to the limited lifetime of plasma-generated radicals and recombination effects.

Contrary, utilizing the thermal ALD process, Zazpe et al. [118] reported uniform ALD deposition of Al_2O_3 coatings within TNT layers with a high AR of ≈180. The conformality of ALD Al_2O_3 coatings with various exposure times of TMA precursor was inspected by SEM at different depth levels of the TNT layers (and supported by in situ QCM measurements and STEM investigations). With an increasing exposure time of TMA, the ALD coating was found to be uniform down to the deepest levels of TNT layers, as shown in Fig. 5a. Optimal exposure time led to uniform coatings within the entire TNT layers, as demonstrated by SEM images measured at four different depth levels of the coated TNT layers, shown in Fig. 5b–e. The observed results correspond to diffusion limited regime of ALD growth, as introduced in [50] and discussed in the previous section.

These pioneering works present the successful utilization of ALD for coating of TNT layers by secondary materials with advanced functionalities, relevant for solar energy conversion and other optoelectronic applications. Obtained results clearly demonstrate that the ultra-thin ALD coating is able to significantly alter the functionality of TNT layers and prove that ALD is the most suitable and practical technique to tailor properties of HAR nanostructures.

Table 1 presents a complete list of reports utilizing ALD for coating HAR anodic TNT layers. In the following text, these reports will be introduced in thematically selected sections, as illustrated in Fig. 1.

4.2. Light absorption and photoelectrochemical conversion

While the TiO_2 efficiently absorbs light in the UV spectral range, the main limitation for solar-light-driven applications of TiO_2 is its relatively large intrinsic band gap (3.2 eV for anatase and 3.0 eV for rutile) which does not allow light absorption within the visible-light spectral range. Besides a dye sensitization [119] or a metal/non-metal doping [120–124], an alternative way to improve visible-light photoelectrochemical (PEC) performance of TiO_2 is the modification of TiO_2 by a suitable narrow band gap semiconductor. The photoexcitation connected with the effective charge separation leading to the electron injection to the TiO_2 conduction band can significantly enhance the visible-light photoresponse of TiO_2 based heterostructures, such as nanoparticulate and nanotubular layers. In order to absorb most of the incident light, the range of thicknesses of the compact absorber layers should be on the microscale. Thus, the ALD does not qualify itself as most suitable deposition technique at first glance for this purpose, since it is technique suitable for production of coatings with thickness on the nanometer scale. However, the situation is diametrically different in the case when HAR nanostructures are used as substrates. Only a few tens of nm thick absorber layer (or even less) are effective enough for efficient solar energy harvesting, as a result of tremendously increased specific surface area of the HAR nanostructure, allowing to reach the effective absorption mass of sensitizer with comparably thinner coatings than for planar substrates, and the multiple light scattering events, prolonging significantly optical path in HAR nanomaterials [125–127]. Moreover, a low thickness of absorber layer is also critical for the reduction of charge recombination losses during charge transfer through the material. The length-scale of effective charge separation is characterized by the size of the depletion layer. On the nanometer scale, the ALD serves as an excellent tool for deposition of uniform coatings with minimum amount of defects, which represents fundamental building block for highly efficient TiO_2 nanomaterials to be used for solar energy conversion applications.

The first work utilizing ALD to coat TNT layers by secondary visible-light absorbing material was carried out by Sarkar et al. [115], as discussed in the previous section. The following work was performed by Huang et al. [128], who deposited Co_3O_4 into TNT layers with AR over 100. The ALD was performed utilizing bis(cyclopentadienyl)cobalt(II) ($Co(Cp)_2$) and O_3 as ALD precursors. The thickness of the coating was ranging up to 20 nm and it was verified by SEM and by the calibration on reference Si wafer. ALD Co_3O_4 coated TNT layers were explored for the visible-light (>420 nm) induced photocurrent generation. The best photocurrent response was observed for TNT layers coated by Co_3O_4 with a thickness of 4 nm. The corresponding PEC performances of the 4 nm ALD Co_3O_4/TNT layer, a reference Co_3O_4/TNT layer coated by impregnation method, and a reference blank TNT layer are shown in Fig. 6a and b. The enhanced PEC performance of ALD Co_3O_4/TNT layers was attributed to the favourable band alignment of Co_3O_4/TNT layers as revealed by XPS, shown in Fig. 6c, and to the ALD technique used, providing uniform Co_3O_4 coating of controlled thickness and with minimal amount of defects, which maintained the large open surface area of TNT layers and minimized charge recombination losses. However, it is worth to note that the reported absolute values of the photoconversion efficiency (Fig. 6b) were extremely low.

A significantly pronounced positive effect on the visible-light photoresponse can be expected, when CdS is utilized as a light

Table 1
Summary of ALD coatings on TNT layers together with the information about geometry of TNT layers (* difference between inner and outer tube diameter taken into account).

	Material	Year	L (μm)	D (nm)	AR	Reference
ALD uniformity	Al_2O_3	2016	20	110	182	[118]
Light absorption	In_2S_3	2010	4	65	62	[115]
	Co_3O_4	2015	10	85	118	[128]
	CdS	2017	0.6	95–56–35	6; 11; 17	[134]
	CdS	2018	1–130	80–230	13–897	[125]
	$MoSeO_x$	2017	5	230	22	[135]
Charge separation	Al_2O_3	2014	23	100	230	[139]
	Al_2O_3	2014	*x*	97	*x*	[140]
	Al_2O_3 + QD	2016	1.7	120	14	[141]
	TiO_2, Al_2O_3, ZnO + QD	2017	1.7	110	15	[142]
	ZnO	2014	4.5	120	38 (*60)	[143]
	ZnO	2014	0.5	60	8	[144,145]
	ZnO + QD	2016	2.4	97	25	[146]
	ZnO	2016	0.5	60	8	[147]
	ZnO + P3HT	2017	0.5	60	8	[148]
	TiO_2	2017	5	230	22	[149]
(Photo)catalysis	Ti, Al, Zn, Sn, Cu, W	2014	7.5	95	79	[175]
	Pd	2015	1	70	14	[172]
	SnO_2 + Pd	2017	1	70	14	[179]
	Pt	2018	7	100	70	[173]
	Pt	2018	1–5–20	80–230–110	13–22–181	[174]
Stability and physical properties	Al_2O_3, TiO_2, Ta_2O_5	2012	1	100	10	[116]
	In_2O_3	2015	0.5–2–8	80–80–100	6–25–80	[117]
	Al_2O_3	2017	20	110	182	[181]
Gas sensing	ZnO	2017	5	230	22	[185]
Energy storage	ZnO Al_2O_3	2013	2	100	20	[200]
	Al_2O_3	2017	5	230	22	[201]

L = tube length; D = inner tube diameter.

absorber with TiO_2 [129]. CdS is predominantly deposited in the form of quantum dots (QD) by conventional techniques such as chemical bath deposition [20,130], successive ionic layer adsorption (SILAR) [21,131], or electrodeposition [132], which can generally provide decoration of HAR nanostructures with much more limited uniformity than ALD. The expected efficiency of CdS sensitized TNT layers scales with the total surface area of TNT layer as long as the TNT layer can be uniformly coated by sensitizer (and diffusion length of charge carriers is long enough to reach collecting electrodes [133]). A direct way to increase surface area (AR) of TNT layers is (i) to decrease the diameter of nanotubes (increase their areal density) or (ii) to increase the overall thickness of TNT layers. The next two works well describe cases (i) and (ii).

Krbal et al. [134] reported downscaling the tube diameter of ALD CdS sensitized TNT layers for efficient PEC energy conversion. TNT layers with thickness of 600 nm and with different average tube diameters of 35, 56, and 96 nm – featuring various surface areas (52, 29, and 23 cm^2/cm^2, respectively) – were coated by 6 nm thick CdS layers by ALD (using dimethylcadmium and H_2S as precursors). The corresponding morphology of CdS coated TNT layers with various tube diameters, captured by SEM, is shown in Fig. 7a–c. The obtained incident photon to conversion efficiencies (IPCE) are shown in Fig. 7d, respectively. The CdS coating of TNT layers led to the strong enhancement of their photoresponse in the visible-light spectral range. The photoresponse rose with the decreasing TNT layer tube diameter (increasing surface area). The composite ALD CdS/TNT layer with the smallest tube diameter ≈ 35 nm (largest surface area ≈ 52 cm^2/cm^2) exhibited IPCE above 50% up to 470 nm with the photoresponse onset around 520 nm (corresponding with the band gap of CdS ≈ 2.4 eV).

In a follow up study, Zazpe et al. [125] presented on the upscaling of the thickness of ALD CdS coated TNT layers. Ultra HAR TNT layers with thicknesses between 1 μm and 130 μm (AR up to 900) were coated by ALD CdS with thicknesses between 2 nm and 10 nm. The evidence of 10 nm CdS coating of a fraction of TNT layer featured by HAADF STEM image and STEM/EDX elemental mapping with corresponding line profiles is depicted in Fig. 7e–g, respectively. The utilization of CdS coated ultra HAR TNT layers resulted first of all into a superior PEC performance, as demonstrated by high IPCE values of around 70%. In addition, it resulted in an apparent shift of the onset of visible-light photoresponse of CdS-TNT layers up to 675 nm (≈1.8 eV, significantly below the band gap of CdS) while the IPCE around 70% was kept in the range from 300 to 600 nm, as it is shown in Fig. 7h. The unexpectedly significant shift of the onset of photoresponse was attributed to the advantageous geometry of the ultra HAR TNT layers giving rise to multiple light-scattering effects, which extremely prolong the optical path of light within nanostructure as illustrated in Fig. 7i and therefore enhances the probability of capturing light by sub-band gap transitions in conformal and uniform ALD CdS coatings. The obtained results clearly demonstrate the profitability of ALD for light harvesting applications to effectively utilize the deposited material in form of a uniform ultra-thin coating, perfectly adopting a large surface/interface area of the support nanostructure, using TNT layer as a model example.

The improved photoresponse of ALD coated TNT layers was also presented by Ng et al. [135], who deposited molybdenum oxyselenide ($MoSe_xO_y$) coating utilizing $Mo(CO)_6$ and $(CH_3Si)_2Se$ ALD precursors. The optimal thickness of the $MoSe_xO_y$ coating for maximal photocurrent generation and photocatalytic degradation of model dye (methylene blue (MB)) was found to be within the range of 2–5 nm. The study represents a fundamental step for future tailored deposition of transition metal dichalcogenides, such as $MoSe_2$ [136], into TNT layers by ALD.

4.3. Charge separation

Generally, one of the key limiting factors of the performance of solar cell devices is the recombination of photogenerated charge carriers. Main charge recombination centres are represented by defects, trap states and charge impurities at surfaces and interfaces,

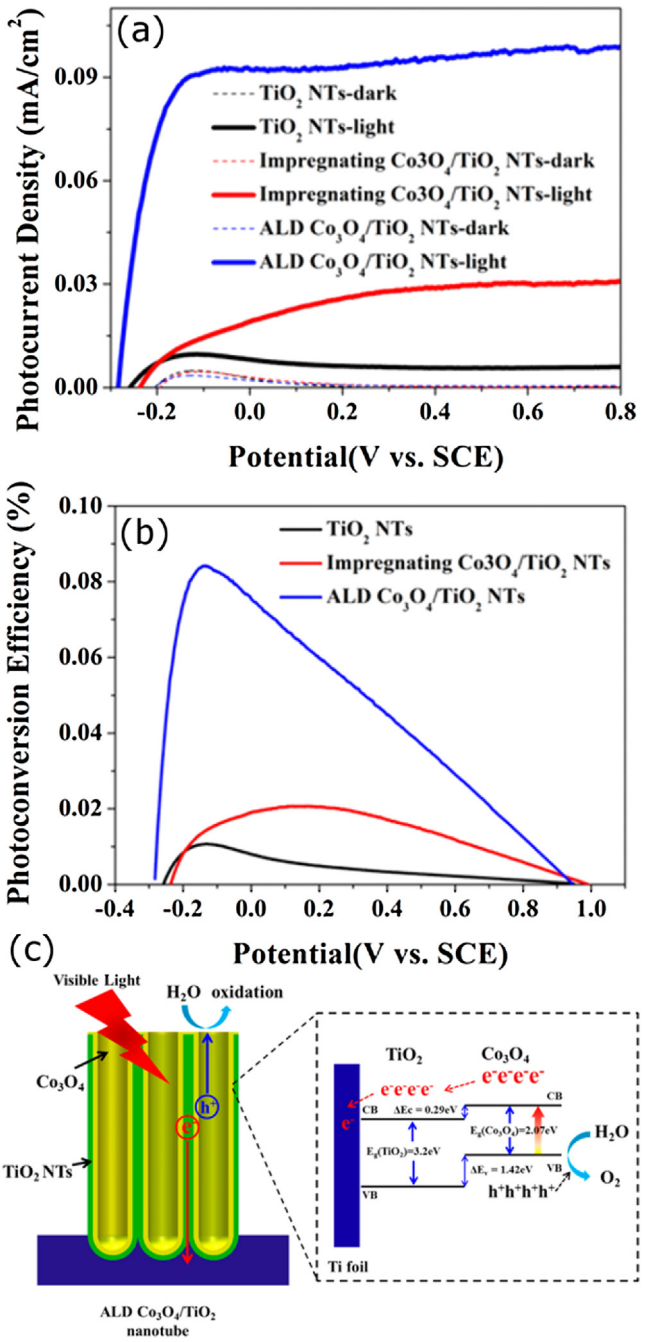

Fig. 6. PEC performance of 4 nm thick Co_3O_4 coating of TNT layers by ALD. (a) The photocurrent density and (b) photoconversion efficiency of Co_3O_4/TNT layer heterostructure upon visible-light illumination (>420 nm, 100 mW/cm^2). (c) Illustration of band alignment within the heterostructure as determined by XPS. Reproduced from [128].

e.g. Ti^{3+} interstitials giving rise to Ti *3d* states below conduction band edge in TiO_2 [137,138]. For HAR nanostructures (which are also high surface area materials), the prevention of recombination at surfaces/interfaces is of utmost importance. One way to suppress the recombination on surface defects is to prepare surfaces with lowest possible concentration of surface defects. This can be realized either by optimization of the growth conditions of that particular material itself or by deposition of an overlayer of a suitable defect-depleted material – passivation layer – which passivates the surface defects of an underlying material. However, such an overlayer should not alter the properties of the underlying material and should be very thin not to limit the charge transfer through the layer itself. The charge recombination at the interfaces can be suppressed by a combination of compatible materials, forming a high quality interface with low amount of defects and with an inherent energy barrier for the back transfer of electrons or holes. ALD, being inherently ideal for the deposition of conformal and uniform coatings with minimal amount of defects and thickness controlled on the nanometer scale, represents very promising technique for the growth of blocking/passivating layers.

The credit of ALD is reflected by a high number of recent studies utilizing ALD for deposition of blocking layers. For the case of TNT layers, the ALD was utilized for the deposition of Al_2O_3 [139–142], ZnO [142–148], and TiO_2 [142,149] thin coatings as blocking layers in order to improve the PEC performance of TNT layers. In addition, the same materials were also utilized as blocking layers in mesoporous TiO_2 layers used in DSSC [150–154].

Wide band gap and almost ideal ALD growth make Al_2O_3 a prototypical material for a blocking layer deposited by ALD. ALD growth of Al_2O_3 is usually realized using TMA and water as precursors. Gui et al. [140] coated TNT layers by Al_2O_3 by 10–200 ALD cycles at 100–400 °C temperature range in order to enhance the PEC water splitting by the surface passivation of TNT layers. The best PEC performance was observed for Al_2O_3 coating by 25 cycles (2.6 nm) at 200 °C yielding 1.8 times higher photocurrent density than bare TNT layers. Kim et al. [139] coated TNT layers with AR of ≈230 by ultrathin Al_2O_3 coatings with thickness of 0.1–0.6 nm (deposited by 1–6 ALD cycles) at 200 °C and subsequently sensitized them with N-719 ruthenium based dye. The study showed that already after one ALD cycle, the Al_2O_3 coating led to an increase of open circuit voltage and prolonged the electron life times. In contrast, Al_2O_3 coatings deposited by more than two ALD cycles was found to reduce the photocurrent density as a result of an increase of the energy barrier for the injection of electrons from the dye to the TiO_2 conduction band. Zeng et al. [141] examined the role of ALD Al_2O_3 overlayers with various thicknesses on PEC performance of coated CdS and PbS QD sensitized TNT layers. The Al_2O_3 overlayers were deposited by 3–100 ALD cycles. The optimal thickness leading to improved charge collection efficiency was found to be 1.5 nm (achieved by 30 ALD cycles) yielding 1.6 times higher photocurrent density than for bare QD sensitized TNT layers. For the illustration of properties of Al_2O_3 ALD coating of TNT layers, the structure of 30 ALD cycles Al_2O_3 coated QD-TNT layers and PEC efficiency with model of beneficial interface band alignment of ALD Al_2O_3 coated QD-TNT layers are shown in Fig. 8a–c.

Fundamental mechanisms behind the passivation effect of Al_2O_3 overlayers can be learned from the field of silicon solar cells [155]. Al_2O_3 coatings help to reduce the surface/interface recombination rate by (i) passivation of surface/interface defects, so-called chemical passivation which is realized by hydrogen incorporated naturally in bulk Al_2O_3 [156] and (ii) by significant reduction of the concentration of one type of charge carrier at the surface/interface by an electric field denoted as field effect passivation, that stems from the inherent accumulation of negative charge in Al_2O_3 near the interface, connected to defects in form of Al vacancies and O interstitials [157]. The higher is the temperature of ALD process, the lower amount of hydrogen is found in Al_2O_3, resulting in less effective chemical passivation [158]. The optimal temperature range for Al_2O_3 ALD deposition is found to be between 150 and 250 °C. The post-deposition annealing of Al_2O_3 improves the passivation effect with onset above 300 °C as it promotes diffusion of H towards the interface and also increases the negative charge accumulated in Al_2O_3. The thickness also affects the passivation capability of Al_2O_3. The chemical passivation starts to be limited for coatings thinner than 5 nm, while the field effect passivation remains down to 2 nm. On the other hand, increased thickness of the passivation layer limits its charge transfer properties. The trade-off between

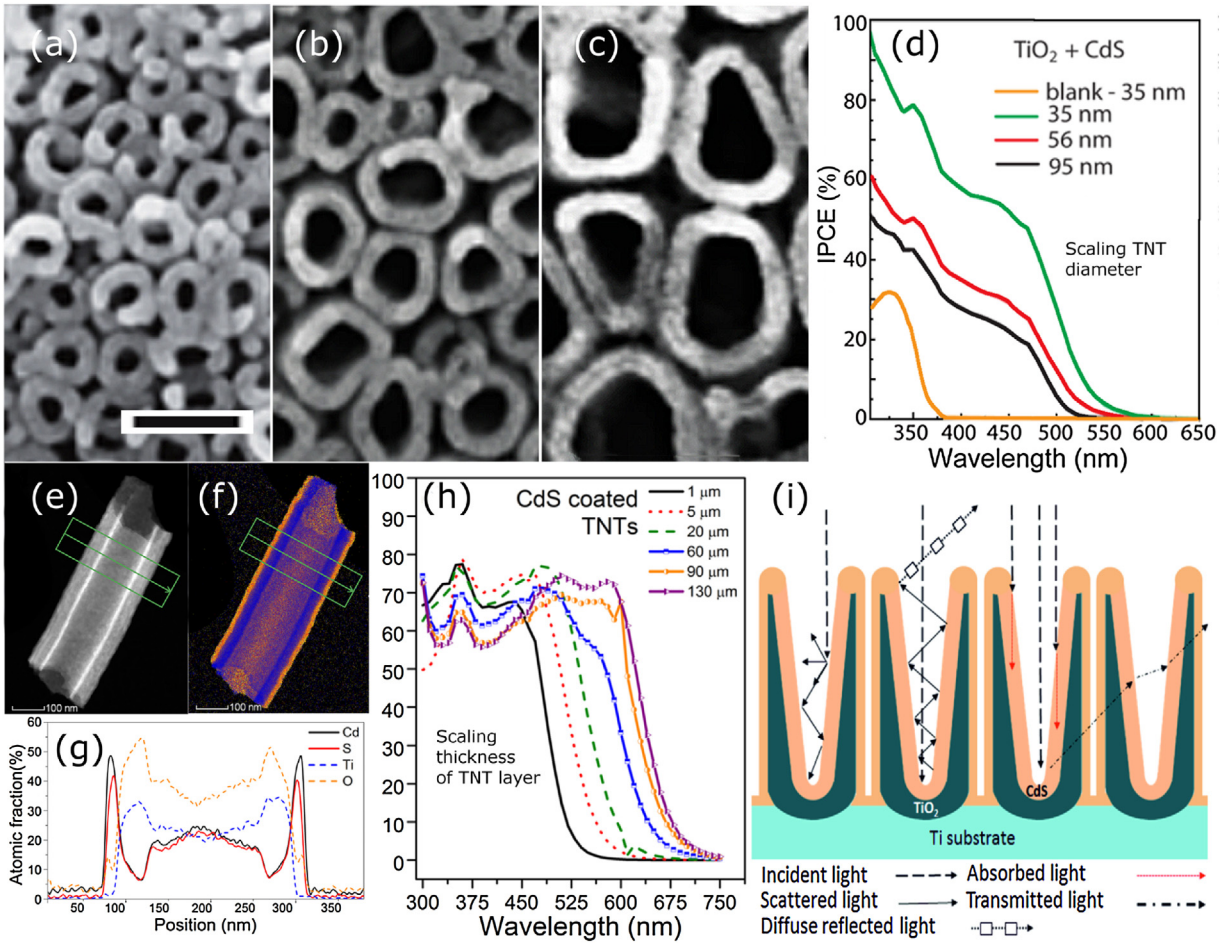

Fig. 7. ALD coating of TNT layers by CdS light-absorber layer for improved visible-light photoresponse. (a–c) SEM images of 6 nm CdS coated TNT layers with average tube diameters 35 nm, 56 nm, and 95 nm, respectively, scale bar 100 nm. (d) IPCE of TNT layers with various nanotube diameter sensitized by 6 nm thick ALD CdS coating upon illumination with a monochromatized light source (e) High angle annular dark field (HAADF) STEM image and (f) STEM/EDX elemental map of fraction of nanotube coated by 10 nm thick CdS overlayer, the green arrows mark the corresponding elemental line profiles shown in (g). (h) IPCE of TNT layers with various thicknesses sensitized by 5 nm thick ALD CdS coating. (i) Illustration of multiple light scattering effects prolonging the optical path of light in TNT layer and facilitating efficient light harvesting. (a–d) Reproduced from [134] and (e–i) reproduced from [125].

the passivation and charge transfer properties yields optimal Al_2O_3 thicknesses of around 2 nm employed as capping passivation layer [155]. The above discussed results clearly demonstrate the uniqueness of ALD to tailor the coatings of HAR nanostructures on atomic level and ultrahigh precision, non-feasible for alternative deposition techniques.

In an analogous way to Al_2O_3, several works addressed to which extent the PEC performance of TNT layers based photoanodes can benefit from the secondary coating by thin ZnO overlayer, deposited by ALD. ZnO represents a direct band gap semiconductor with the band gap value (3.4 eV) close to TiO_2, which is known to promote efficiency of DSSC [159]. Jeong et al. [143] coated TNT layers by 10 nm thick ZnO (using 50 ALD cycles) and sensitized it by N719 dye. The ZnO coating was found to form a particulate-like decoration of TNT layers increasing the surface area of the photoanode. The short circuit photocurrent density improved from 3.98 to 4.31 mA/cm^2. Correspondingly, the efficiency improved from 1.23 to 1.42% by ZnO coating. The positive effect of the ZnO coating was attributed to the increased surface area of ZnO coated TNT layers and to the high isoelectric point of ZnO forming an inherently positive charge at the ZnO/electrolyte interface, facilitating an efficient dye adsorption. Moreover, the difference of TiO_2 and ZnO isoelectric points caused a negative shift of the TiO_2 conduction band, resulting in an increased energy level difference with the liquid electrolyte leading to an increased open circuit voltage.

In several studies, Cai et al. [144,145,147,148] inspected the effect of 2, 5, and 10 nm thick ZnO coating (deposited by 10, 25, and 50 ALD cycles) on the PEC performance of ZnO/TNT layers and of functionalized poly(3-hexylthiophene)/ZnO/TNT layers. The best PEC performance was revealed for 2 nm thick ZnO film (10 ALD cycles). The photocurrent density rose by a factor of 1.6 and the results of impedance spectroscopy pointed to the improved charge separation featured by lowered charge-transfer resistance, negative shift of flat band potential, and longer electron lifetimes. The additionally poly(3-hexylthiophene) functionalized ZnO/TNT layers showed increased light absorption and promoted photoluminescence quenching as a mark of supressed radiative recombination of photogenerated charge carriers [148].

Zeng et al. [146] deposited a thin ZnO layer by ALD as an interlayer for PbS and CdS QD sensitized TNT layers. The authors utilized TNT layers with various thicknesses (1.5–2.8 μm) and coated them by ALD ZnO with thickness between 0.7 and 10.5 nm (5, 10, 30, and 70 ZnO ALD cycles). The ALD ZnO/TNT layers were afterwards loaded by CdS/PbS QD using SILAR technique. Illustrative SEM and TEM images of TNT layer coated by ALD ZnO (30 ALD cycles equivalent to thickness of 4.5 nm) and decorated by PbS/CdS QD are shown in Fig. 8d and e. The observed increase of the light absorption and the PEC performance after ZnO coating was most pronounced for the 2.4 μm thick TNT layers with CdS/PbS QD loaded over coating of 10 ALD cycles of ZnO (1.5 nm thick) resulting in the maximum

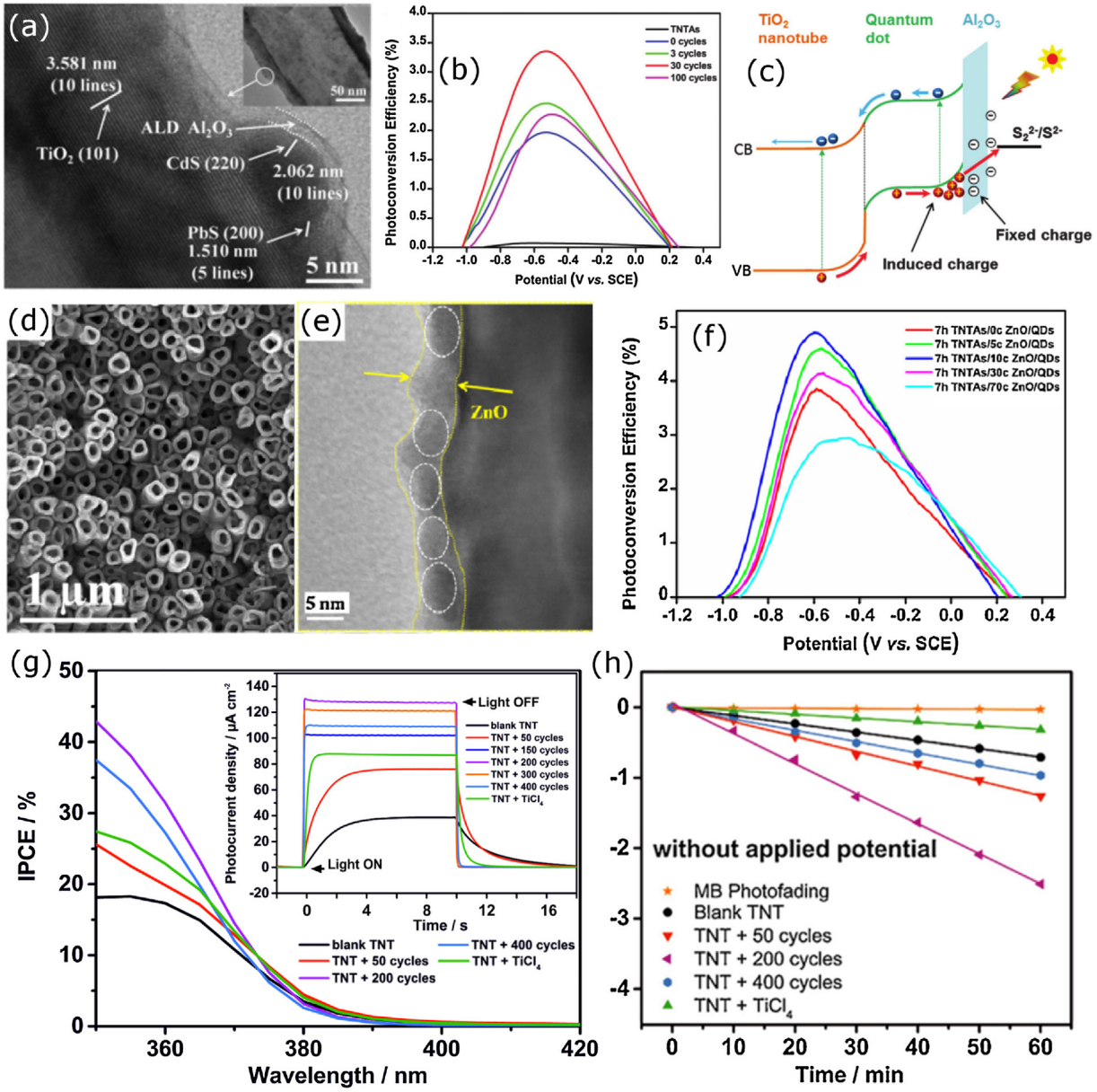

Fig. 8. ALD deposited surface passivation layers for enhanced charge separation. (a) Representative TEM image, (b) observed PEC efficiency, and (c) model of interface band alignment of ALD Al_2O_3 passivated QD sensitized TNT layers, adopted from [141]. (d) SEM top view, (e) TEM side view, and (f) PEC efficiency of ALD ZnO coated QD sensitized TNT layers, reproduced from [146]. (g) IPCE and (h) rate of photocatalytic decomposition of model dye by ALD TiO_2 passivated TNT layers, reproduced from [149].

photoconversion efficiency of 4.6% at −0.6 V (1.3-fold increase compared to uncoated PbS/CdS QD sensitized TNT layers), as shown in Fig. 8f. The positive effect of ZnO interlayer was rather attributed to the increased amount of QD formed on ZnO modified TNT layers, than to effective passivation/blocking properties of ZnO coating. The ZnO coating itself was not found to alter the PEC properties of TNT layers. This was attributed to the amorphous structure of ZnO coatings leading to significant recombination of photogenerated charge carriers.

Generally, ZnO is considered as an attractive material for the coating of photoanodes because of its high electron mobility, which is at least an order of magnitude higher than in TiO_2 [160]. However, the high electron mobility in ZnO is also accompanied by a high recombination rate of charge carriers, limiting the overall PEC performance of any potential application. Contrary to Al_2O_3, neither the direct evidence of passivation effect of ZnO overlayers, nor the underlying fundamental process in a strict sense of chemical or field effect passivation have been introduced for ZnO coatings of TNT layers. The pronounced effects of ZnO coatings on PEC performance can be attributed to a higher uptake of dye molecules, higher electron mobility, and an increase of the open circuit voltage due to staggered band alignment in ZnO/TiO_2 heterostructures [142–148]. ZnO features itself rather as an electron transport layer, which can in combination with TiO_2 boost electron transport properties, rather than a typical blocking layer forming an energy barrier supressing the charge recombination.

One of the key attributes of ALD is the deposition of high quality thin films with low concentration of defect sites and absence of pinholes. Therefore, it can be beneficial to coat TiO_2 nanostructures by additional ALD TiO_2 coatings. TiO_2 ALD coating of TiO_2 nanowires and nanorods leads to significantly improved PEC performance attributed to improved charge collection efficiency by passivation of defect sites and increased surface area [161,162]. Anodized TNT layers produced in ethylene glycol based electrolytes

are known to form a double wall structure with a porous inner wall rich on carbon and Ti-oxyhydroxide species, which limit the electron transport properties [14,163]. The removal of the inner wall improves the carrier transport [164], photocatalytic [165], and PEC properties of the TNT layers [166] and leads to a better performance of TNT layers in DSSC [147]. However, it requires the double wall TNT layers to be etched in piranha solution to remove the inner wall. Another approach is to coat the double wall TNT layers with TiO_2 by ALD. Sopha et al. [149] presented enhanced PEC performance of anodized TNT layers coated by ALD TiO_2 overlayers with various thickness ranging from 3 to 22 nm (50 to 400 ALD cycles). The PEC performance of ALD TiO_2 coated TNT layers was compared to blank TNT layers and TNT layers decorated with TiO_2 nanoparticles deposited from $TiCl_4$ solution. The obtained IPCE and photocatalytic degradation of a model dye (MB) are shown in Fig. 8g and h, respectively. The presence of the coating led to an increase of the photocurrent density and more effective dye decomposition. The coating with optimal thickness, corresponding to 11 nm (200 ALD cycles), displayed two fold increase of photocurrent density over blank TNTs layers, 1.5 times higher photocurrent density than nanoparticle decorated TNT layers, and 3.5 times higher rate constant for MB decomposition. Moreover, a significantly decreased amount of trap states in TiO_2 as a results of ALD TiO_2 coating of TNT layers was stressed out by a significantly faster photocurrent response in the photocurrent transients for TiO_2 coated TNT layers in comparison to uncoated ones. These data were corroborated with Mott–Schottky measurements showing lower majority charge carrier concentration pointing to decreased defect and oxygen vacancy concentrations in ALD TiO_2 coatings. Thicker TiO_2 coatings led to partial clogging of tube interiors and to a decrease of the active surface area and hence lower PEC activity.

Zhou et al. in 2017 [142] performed a cross comparison of the effect of 1.5 nm thick TiO_2, ZnO, and Al_2O_3 passivation ALD coatings on PEC performance of PbS/CdS QD sensitized (using SILAR) TNT layers. The maximal photocurrent densities were found to be 4.3, 5.0, 5.6 mA/cm^2 for TiO_2, ZnO, and Al_2O_3 overlayers, respectively. In line with previous work [141], the coating by Al_2O_3 was found to be able (i) to increase the charge carrier concentration by passivation of surface trap sites and (ii) to improve the charge transfer efficiency in the bulk and at the interface while the ZnO and TiO_2 coatings were found only to improve the charge transfer efficiency.

4.4. Photocatalysis and electrocatalysis

TiO_2 represents one of the important building blocks for advanced catalytic materials for fuel and chemicals processing, hydrogen economy, and water/environmental remediation processes [167]. Photocatalytic and electrocatalytic applications of anodic TNT layers benefit from high surface area, improved charge separation and efficient charge transfer properties of TNT layers [168]. Another important aspect is also that the anodic TNT layers are inherently firmly attached to the metal Ti support, giving lots of advantages. As compared with nanoparticles, there is no immobilization pre-treatment or separation post-treatment needed for direct catalytic applications of anodic TNT layers. In order to develop even more effective TNT layer-based photocatalysts or electrocatalysts, it is of advantage to combine TNT layers with functional secondary materials in the form of compact coatings or nanoparticles [169–174]. As emphasized earlier in the text, ALD represents an ideal technique for coating of HAR nanostructures featuring high uniformity, low amount of defects, and a high degree of control over deposition rate. For the photocatalytic applications based on TNT layers, it is important to stimulate visible-light photoresponse, facilitate adsorption of reactants and desorption of products, and improve charge transfer to reactants. For the electrocatalytic applications, the TiO_2 plays the role of the metal oxide support facilitating good particle dispersion all around the surface and promoting the stability of metal particle catalysts [174].

The first work employing ALD for promoting photocatalytic properties of TNTs layers was introduced by Turkevych et al. [175]. The authors explored the synergistic effect between TiO_2 and metal oxide/sub-oxide/mixed-oxide nanoclusters on the photocatalytic decomposition of MB under simulated solar light. TNT layers with a thickness of 7.5 μm and tube diameters of 95 nm were loaded by Al_2O_3, SnO_2, TiO_2, ZnO, CuO, and WO_3 (employing water as the oxidant, total 6 ALD cycles), their sub-oxides (employing atomic hydrogen, total 3 ALD cycles), and mixed oxides. Resulting rate constants of MB decomposition for ALD functionalized TNT layers (relative to the bare TNT layer and compared to TNT layers functionalized by chemical bath deposition (CBD)) are shown in Fig. 9a. Modification of TNT layers by stoichiometric metal oxides did not lead to an increase of the photoresponse, while for the metal suboxides and mixed oxides the significant synergy led to an increased photoresponse. The positive effect on the visible-light absorption was attributed to the upward shift of the valence band of TiO_2 (without an effect on the conduction band) near the surface induced by the presence of suboxide/mixed oxide clusters, featuring low valence states [176] and metal-to-metal bonds at non-stoichiometric interfaces between agglomerated suboxide/mixed oxide nanoparticles [177].

Another possibility to prepare catalytically active TNT layers is to decorate them with noble metal nanoparticles. Assaud et al. [172] deposited Pd nanoparticles by ALD into TNT layers for electrooxidation of ethanol (EOR). ALD was employed to allow a precise control over the deposition rate of Pd and to provide uniform size distribution of particles over the entire TNT layer surface. Various Pd nanoparticles with sizes from 6.5 to 25 nm (400–900 ALD cycles) were deposited on as-anodized (amorphous) and annealed (450 °C, anatase) 1 μm thick TNT layers with a tube diameter of 70 nm, which were anodized in an aqueous F^- electrolyte. Cyclic voltammetry and chronoamperometry revealed the best electrocatalytic performance and satisfactory stability for Pd nanoparticles with an average size of 7 nm (500 ALD cycles) deposited within annealed TNT layers. Negligible electroactivity of smaller Pd particles was attributed to strong metal-support interaction [178], resulting in burying of Pd nanoparticles into the TiO_2 support and their deactivation. On the other hand, lower electroactivity of larger Pd particles was attributed to very weak metal support interaction and a decreased surface area. Annealing of TNT layers was found to stabilize Pd in the metallic state (the active form for the ethanol electroxidation) and to increase the electron conductivity.

Follow up work of Barr et al. [179] studies the effect of ALD coated SnO_2 TNT layers as a support loaded by ALD deposited Pd nanoparticles on the electroactivity for EOR. ALD was first utilized for coating TNT layers with SnO_2 as a support for later ALD deposition of Pd nanoparticles. It is worth to note that the nucleation period of the Pd ALD growth on ALD SnO_2 modified TNT layers (less than 100 cycles) was found to be comparably lower than on bare TNT layers (400 ALD cycles), as a result of strong reduction of SnO_2 surface during Pd deposition by ALD. The morphology of the Pd/SnO_2/TNT composite structure is illustrated schematically in Fig. 9b. The TEM image reveals structure of ALD 6.5 nm Pd nanoparticles/ALD 14 nm (annealed) SnO_2/TNT layer, which displayed the best electrocatalytic activity for EOR, as depicted in Fig. 9c. The promotional effect of SnO_2 on catalytic activity of Pd nanoparticles was attributed to (i) facilitated OH adsorption on SnO_2, (ii) favourable Pd nucleation and ALD growth on SnO_2, (iii) higher electrical conductivity of annealed SnO_2, and (iv) metal–support interaction.

Photocatalytic generation of hydrogen by ALD Pt loaded TNT layers was demonstrated by Yoo et al. [173]. Single walled TNT layers [163] were exposed to different number of Pt ALD cycles (8–72

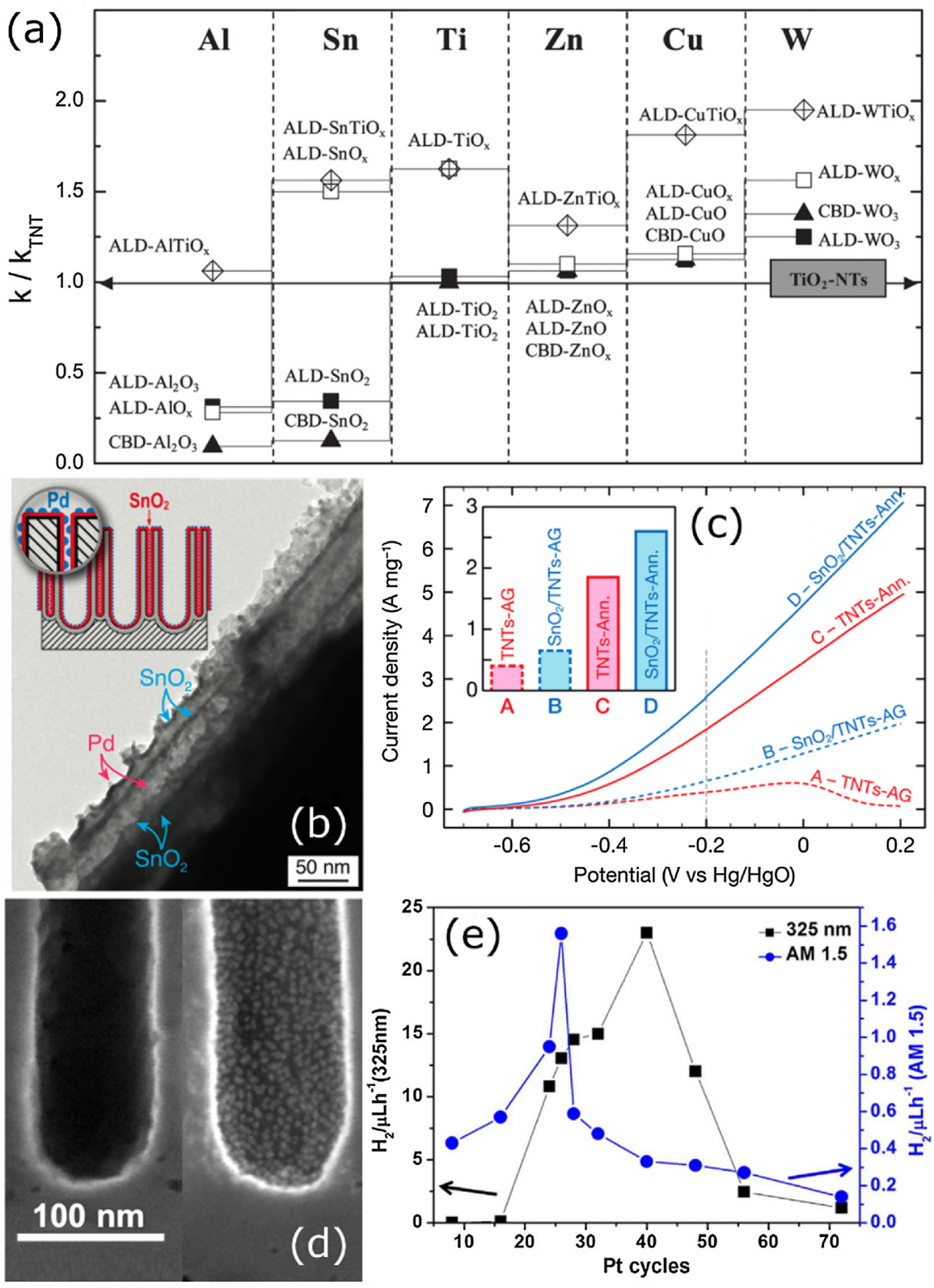

Fig. 9. ALD functionalized TNT layers for photocatalytic and electrocatalytic applications. (a) Relative rate constants of methylene blue decomposition on TNT layers coated by various ALD and CBD deposited metal oxides/suboxides/mixed oxides, reproduced from [175]. (b) TEM image of ALD Pd nanoparticles on a ALD SnO_2 coated TNT layer for ethanol electrooxidation, composite nanostructure is illustrated schematically in the inset. (c) Linear sweep voltammetry and photocurrent density at −0.2 V (inset) for 500 cycles Pd on as-grown TNTs, annealed TNTs, as-grown SnO_2/TNTs, and annealed SnO_2/TNTs in 1 M KOH + 1 M C_2H_5OH, scan rate 25 mV/s. (b) and (c) were reproduced from [179]. (d) SEM picture of bare and 40 ALD cycles coated TNT and (e) corresponding dependence of photocatalytic H_2 generation yield on Pt-ALD loading cycles under UV light (left) and solar light (right). (d) and (e) were reproduced from [173].

cycles) leading to the growth of Pt nanoparticles with diameter of 2–15 nm. The morphology of bare and Pt-TNT layers loaded by 40 ALD cycles is shown in Fig. 9d, where the homogeneous coating of nanotube's bottoms by uniform Pt nanoparticles (11 nm) is evident. Photocatalytic generation of hydrogen by Pt-TNT layers with different Pt loading upon illumination by UV laser (235 nm) and solar simulated light is shown in Fig. 9e. Pt plays the role of the co-catalyst enabling efficient electron transfer at the catalyst/environment interface. The best performance is observed for Pt particles with a size of 7 nm (26 cycles, highest areal density) and 11 nm (40 cycles) for simulated solar light and UV illumination, respectively. The difference of these maxima is attributed to the light penetration depth, i.e. result of a trade-off between the positive effect of Pt loading and the negative effect caused by shading of TiO_2 support.

Another utilization of ALD Pt nanoparticles modified TNT layers for electrocatalytic methanol oxidation was reported by Anitha et al. [174]. Methanol oxidation reaction is crucial for the operation of the anode side of direct methanol fuel cells [180]. TNT layers with different thicknesses (1, 5, and 20 μm) were coated by Pt particles with average diameters ranging from 1.3 to 4.6 nm (and continuous Pt film). The best electrocatalytic performance (showing 74 mA/cm^2 anodic current density with superior time stability) was reported for 20 μm thick TNT layers decorated by Pt particles with average size 4.6 nm (88 ALD cycles). The obtained results were outperforming the classical substrates used for electrocatalysis, such as graphite or carbon Pt black. The high electrocatalytic activity was attributed to the Pt–TiO_2 metal–support interaction, preventing CO poisoning of Pt particles and the effective utilization of high surface area of TNT layers as a support for homogeneously distributed active Pt nanoparticles provided by ALD.

4.5. Stability and improved physical properties

In addition to the enhanced charge carrier separation, light absorption and (photo)catalytic properties discussed above, ALD coating of TNT layers by secondary materials brings also the possibility to improve mechanical, thermal, and chemical stability of TNT layers. Enhanced mechanical stability of TNT layers can, for instance, help to boost applications of modified TNT layers as flow-through membranes for photocatalysis [13] or those, where some wear (friction) can be expected. On the other hand, the thermal and chemical stability are important for utilization of TNT layers for catalytic and gas sensing applications at elevated temperatures and in harsh acidic environments (ambient humidity).

Positive effects of ALD Al_2O_3 coatings (1–42 nm thick) on the stability of TNT layers were reported by Zazpe et al. [181]. Therein, ALD Al_2O_3 coatings as thin as 1 nm led to an increased thermal stability of the TNT layers up to 870 °C in air (nanotubular structure was preserved) and provided extremely good chemical stability of TNT layers in strongly acidic environments (solution of H_3PO_4 at 60 °C), while the bare TNT layers collapsed, as depicted in Fig. 10a–d. The Al_2O_3 overlayer was found to help to maintain the TiO_2 anatase crystal structure (more favourable for electron transfer) over wider range of temperatures, blocking the conversion to TiO_2 rutile as a result of hindered oxygen diffusion through Al_2O_3 coating. Moreover, Al_2O_3 coating of TNT layers improved the mechanical integrity of TNT layers, as determined by nanoindentation measurements depicted in Fig. 10e, respectively. In the already discussed work of Zeng et al. [141], 1.5 nm thick ALD Al_2O_3 coating was found to effectively retard the photocorrosion of chalcogenide QD used as a sensitizer of TNT layers, as it is illustrated on photocurrent decay in Fig. 10f.

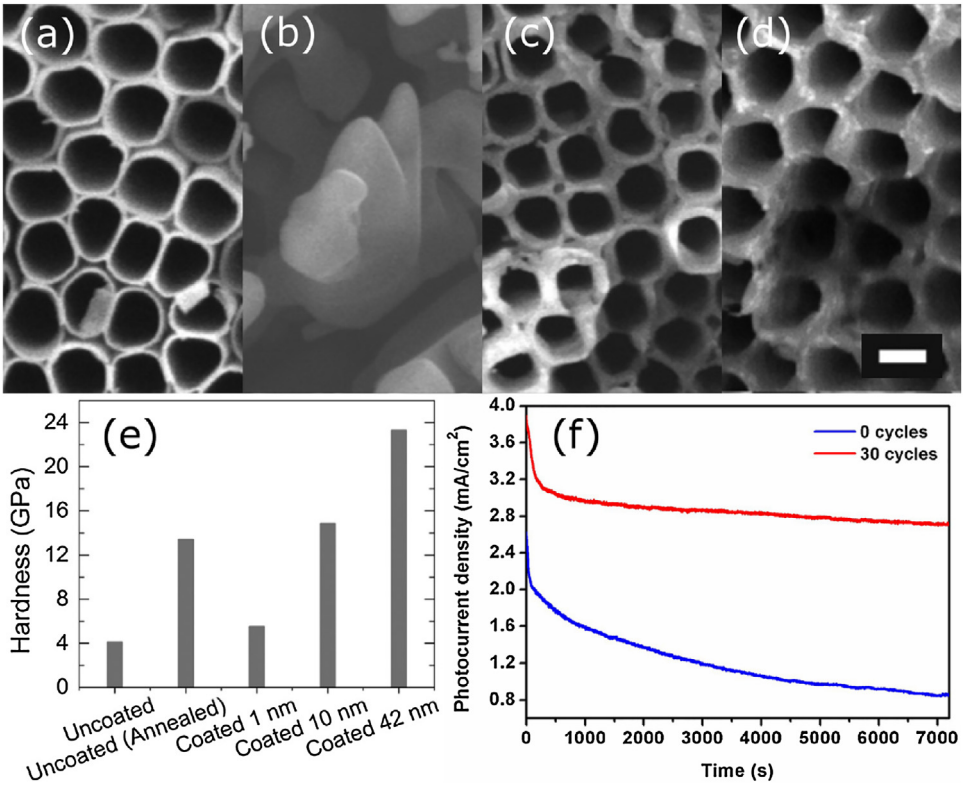

Fig. 10. Improved stability of TNT layers coated by ALD Al_2O_3. (a) As prepared bare anodic TNT layer which (b) collapsed as a result of annealing at 870 °C in air. (c) Preserved structure of 1 nm thick ALD Al_2O_3 coated TNT layer upon annealing at 870 °C and (d) soaking in a solution of H_3PO_4 (85 wt%, 60 °C, 8 h), size of scale bar is 100 nm (representative for all SEM images). (e) Improved mechanical integrity of ALD Al_2O_3 coated TNT layer. (a–e) reproduced from [181]. (f) Higher resistivity of QD sensitized TNT layer to photocorrosion as a result of surface passivation by 1.5 nm thick ALD Al_2O_3 layer, reprinted from [141].

4.6. Gas sensing

TNT layers as a 1-D material with a high surface to volume ratio represent promising nanostructures for the utilization in gas sensors [182,183]. 1-D nanostructures are suitable for conductometric gas sensors, which are based on the change of resistivity with the adsorption of target-detection gases. The adsorption of gas influences the conductivity only in the near surface region and therefore for high response/low detection limit it is necessary to build gas sensors with maximal surface to volume ratio. The best sensitivity can be achieved, if the size of the gas sensing nanostructure is constrained to the size of the charge depletion layer (typically tens of nanometers). The high quality uniform coatings produced by ALD in HAR nanostructures (such as TNT layers), with thicknesses adjustable on the nanometer scale, represent an excellent way to tailor the sensitivity and selectivity of 1-D nanostructured (TNT layers-based) gas sensors [184].

Ng et al. reported a successful utilization of ALD for modification of TNT layers by thin ZnO coatings for ethanol sensing [185]. TNT layers were coated by ZnO overlayers with thicknesses ranging from 0.2 to 19 nm. Interestingly, the ZnO coatings were shown to increase the photoresponse of TNTs layers in the UV spectral range and to extend it towards visible spectral range, as illustrated in Fig. 11a. The best performance was recorded for 19 nm thick ZnO coating, possessing nearly 90% (bias voltage assisted) conversion of photons to electrons in the UV spectral range. In line with the results discussed above, the improved PEC performance of ZnO coated TNT layer was attributed to (i) advantageous TiO_2/ZnO heterojunction structure promoting charge generation and separation, (ii) surface passivation of surface traps of TNT layers, and (iii) reduced depletion width at electrolyte/ZnO interface as a result of UV light stimulated oxygen desorption [186] and applied bias voltage.

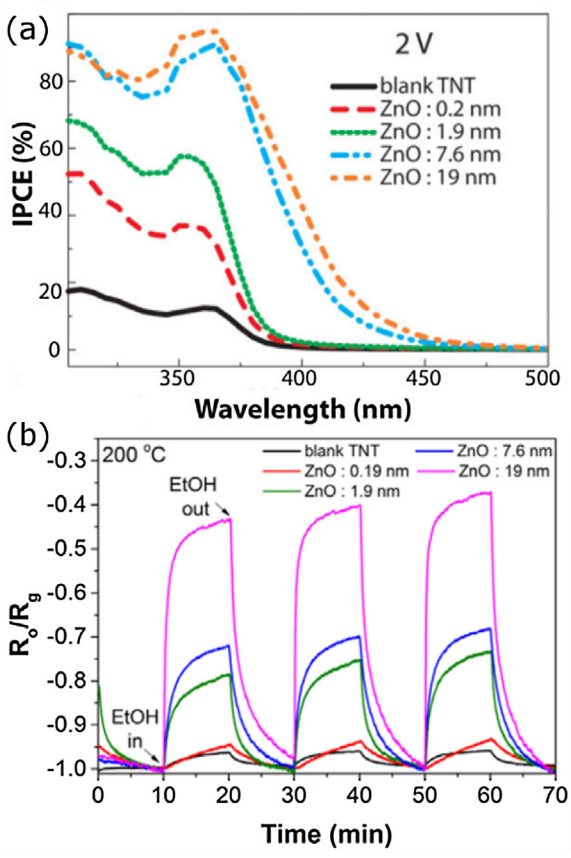

Fig. 11. (a) Incident photon to electron conversion efficiency and (b) resistivity response upon exposure to ethanol of ALD ZnO coated TNT layers. Reproduced from [185].

Sensing responses of ALD ZnO coated TNT layers towards ethanol at 200 °C are shown in Fig. 11b. The ZnO coating led to a significant response to 1930 ppm of ethanol. The best performance was observed for 19 nm thick ZnO coating. The sensing mechanism of ZnO coated TNT layers was explained by the surface depletion model [187]. Thus, in the initial high resistance state, the ZnO surface is depleted of electrons as a result of trapping of electrons by oxygen adsorbates. The drop of resistance upon exposure to ethanol was associated to an interaction between adsorbed oxygen species and ethanol leading to the release of oxygen-trapped electrons to the conduction band of ZnO.

ALD demonstrated to support realization of a functional gas sensor, based on the coating of HAR nanostructures (TNT layers) acting as a sensor scaffold. ALD provides the possibility to boost the sensitivity of gas sensors by conformal deposition of functional secondary materials into high surface area TNT layers and the synergy of functional properties by fine tuning of the thickness of secondary material and its interface with the TNT layers. Moreover, in an analogous way to ref [188], the selectivity of ALD-TNT layers based gas sensor can be potentially tuned by deposition of multiple secondary materials. These can coat various depth levels of TNT layers as a result of sequential ALD process, employing various exposure times for control of the diffusion length of the particular precursors.

4.7. Energy storage

Besides the above mentioned applications, TiO_2 (anatase) is considered to be an interesting material for the negative electrode of Li-ion batteries thanks to its ability to insert Li ions (TiO_2 inserts up to 0.5 Li^+ ions per structure unit), enhanced safety operation, low self-discharge, good capacity on retention, and high power density [189–192]. Utilization of nanostructured TiO_2, in particular anodic TNT layers, brings benefits of higher energy/power densities because of the higher surface area, shorter ion diffusion lengths between electrodes, improved electron transfer, and better accommodation of volumetric changes during the charge/discharge cycles [193–195]. The unique property of ALD to provide high-quality coating of nanostructured materials brings the opportunity to design complex electrodes for the best device performance. ALD can assist to develop a stable solid/electrolyte interface layer with high ionic conductivity and mechanical integrity [35,196–199].

The first application of ALD for modification of TNT layers for Li-ion batteries was reported by Li et al. [200], who coated TNT layers by ZnO (no details about the thickness of the coating or its uniformity were provided). ZnO is a material with high theoretical charge capacity (978 mAh/g) as compared to the charge capacity of TiO_2 (168 mA/h), but poor cycling ability because of high volumetric changes during charge–discharge cycles. However, as reproduced in Fig. 12a, the study showed that ZnO ALD coated TNT layers exhibit two times higher capacity than the bare counterparts and the overall performance of ALD ZnO coated TNTs layers was maintained upon 200 charge-discharge cycles. The improved performance was attributed to the synergy between the ALD ZnO coating, providing higher charge capacity and easier ion diffusion, and the TNT layers that accommodate volumetric changes during charge–discharge cycling.

Alternatively, Sopha et al. [201] inspected the effect of ALD Al_2O_3 coating of TNT layers on their performance as anode in Li-ion batteries. Al_2O_3 was deposited by the well-established ALD process used previously [118,181], leading to uniform coatings with thicknesses controlled on the atomic level (as discussed above), in this case ranging from 0.2 to 10 nm. The best charge capacity was observed for TNT layers coated by 1 nm thick Al_2O_3, while thicker coatings showed reduced capacity. The discharge capacity of 1 nm Al_2O_3

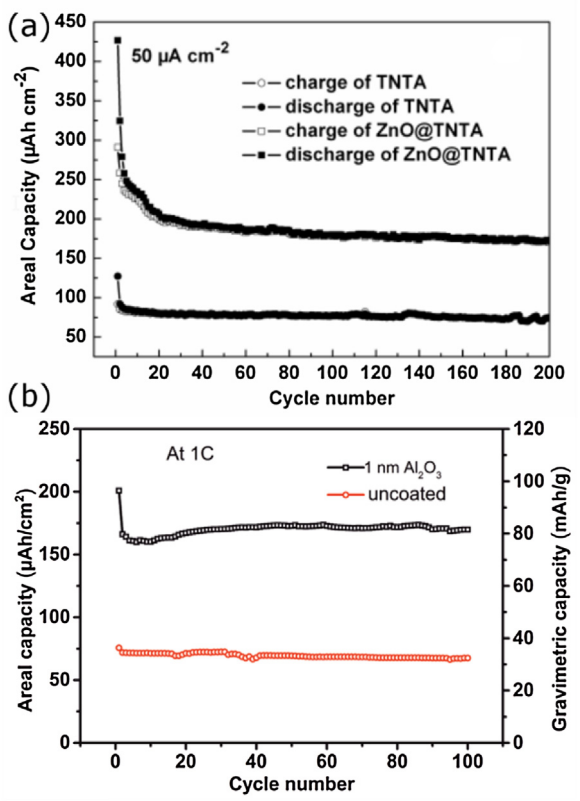

Fig. 12. (a) Charge/discharge capacity of bare and ALD ZnO coated TNT layer as a function of charge/discharge cycles, reproduced from [200]. (b) Improved charge capacity of ALD Al_2O_3 coated TNT layer as compared with uncoated TNT layers throughout multiple charge/discharge cycles, reproduced from [201].

coated TNT layers (at 1C rate) as a function of number of discharge cycles is shown in Fig. 12b. No mark of drop of charge capacity was observed through 100 discharge cycles. The enhanced charge capacity and the stability during charge/discharge cycling were attributed to (i) the better diffusion of Li^+ ions (through <1 nm thick Al_2O_3 layer) as a result of the formation of a surface Li–Al–O phase and (ii) the improved mechanical integrity of coated TNT layers (as demonstrated in [181]), leading to better accommodation of volumetric changes during cycling.

5. Conclusion

ALD represents an exceptional method for tailoring the functionality of nanostructured materials for various energy-related applications. The principal benefit of ALD over other techniques is its ability to provide conformal and uniform coatings of complex nanostructured materials, including HAR materials, with atomic scale thickness control and minimum amount of defects and pinholes. ALD enables the combination of materials within porous nanostructures with unequivocal precision. The utilization of ALD for coating of TNT layers allows to extend the existing broad range of benefits of TNT layers to novel functionalities and applications of resulting heterostructures. Based on the herein reviewed reports, it is clear that the functionality of TNT layers can be completely altered already upon coating by secondary material with a thickness of only a few nanometers (or even less). In general, ALD coatings of TNT layers can significantly improve their chemical, mechanical, and thermal stability. A pathway to the competitive performance of TNT layer-based solar cells and photocatalysts can be paved away by ALD coatings of secondary materials for an efficient visible-light absorption, improved charge separation, and lowered charge recombination. Likewise, the catalytic properties of TNT layers can be advanced by ALD deposition of noble metal nanoparticles, leading to the formation of homogeneously distributed metal nanoparticles (strongly attached to TNT walls) with narrow particle size distribution. Regarding the application of TNT layers in gas sensors, ALD brings the opportunity to deposit functional secondary coatings with adjusted thickness for the best sensor sensitivity and selectivity. In energy storage applications of TNT layers, the ALD allows to deposit conformal coatings for improved ion transport and ion insertion properties and to design solid/electrolyte interface for long-term cycling stability.

The potential of ALD for functionalization of anodic TNT layers remains still relatively unexplored. For the future work, it is necessary to utilize a broader range of ALD compatible functional secondary materials and move towards the design of complex HAR heterostructures, seeking for emerging and new synergic properties.

Acknowledgements

European Research Council (project nr. 638857), Ministry of Youth, Education and Sports of the Czech Republic (projects nr. LM2015082, LQ1601) and Czech Science Foundation (project nr. 18-03881S) are acknowledged for financial support of this work. We thank Dr. Veronika Podzemna and Dr. Jan Michalicka for SEM and TEM analyses, respectively. We thank Dr. Anitha Veettikkunnu Chandran, Dr. Sayantan Das and Dr. Martin Motola for their valuable support for some of the papers reviewed here.

References

[1] A. Fujishima, K. Honda, Electrochemical photolysis of water at a semiconductor electrode, Nature 238 (1972) 37–38, http://dx.doi.org/10.1038/238037a0.
[2] X. Chen, S.S. Mao, Titanium dioxide nanomaterials: synthesis, properties, modifications and applications, Chem. Rev. 107 (2007) 2891–2959, http://dx.doi.org/10.1021/cr0500535.
[3] Z. Fei Yin, L. Wu, H. Gui Yang, Y. Hua Su, Recent progress in biomedical applications of titanium dioxide, Phys. Chem. Chem. Phys. 15 (2013) 4844, http://dx.doi.org/10.1039/c3cp43938k.
[4] A.S. Aricò, P. Bruce, B. Scrosati, J.-M. Tarascon, W. van Schalkwijk, Nanostructured materials for advanced energy conversion and storage devices, Nat. Mater. 4 (2005) 366–377, http://dx.doi.org/10.1038/nmat1368.
[5] U. Diebold, The surface science of titanium dioxide, Surf. Sci. Rep. 48 (2003) 53–229, http://dx.doi.org/10.1016/S0167-5729(02)00100-0.
[6] B. O'Regan, M. Grätzel, A low-cost, high-efficiency solar cell based on dye-sensitized colloidal TiO_2 films, Nature 353 (1991) 737–740, http://dx.doi.org/10.1038/353737a0.
[7] A. Kojima, K. Teshima, Y. Shirai, T. Miyasaka, Organometal halide perovskites as visible-light sensitizers for photovoltaic cells, J. Am. Chem. Soc. 131 (2009) 6050–6051, http://dx.doi.org/10.1021/ja809598r.
[8] X. Gao, J. Li, J. Baker, Y. Hou, D. Guan, J. Chen, C. Yuan, Enhanced photovoltaic performance of perovskite $CH_3NH_3PbI_3$ solar cells with freestanding TiO_2 nanotube array films, Chem. Commun. 50 (2014) 6368–6371, http://dx.doi.org/10.1039/C4CC01864H.
[9] X. Wang, Z. Li, J. Shi, Y. Yu, One-dimensional titanium dioxide nanomaterials: nanowires, nanorods, and nanobelts, Chem. Rev. 114 (2014) 9346–9384, http://dx.doi.org/10.1021/cr400633s.
[10] K. Lee, A. Mazare, P. Schmuki, One-dimensional titanium dioxide nanomaterials: nanotubes, Chem. Rev. 114 (2014) 9385–9454, http://dx.doi.org/10.1021/cr500061m.
[11] J.M. Macak, H. Tsuchiya, A. Ghicov, K. Yasuda, R. Hahn, S. Bauer, P. Schmuki, TiO_2 nanotubes: self-organized electrochemical formation, properties and applications, Curr. Opin. Solid State Mater. Sci. 11 (2007) 3–18, http://dx.doi.org/10.1016/j.cossms.2007.08.004.
[12] F. Riboni, N.T. Nguyen, S. So, P. Schmuki, Aligned metal oxide nanotube arrays: key-aspects of anodic TiO_2 nanotube formation and properties, Nanoscale Horiz. 1 (2016) 445–466, http://dx.doi.org/10.1039/C6NH00054A.
[13] S.P. Albu, A. Ghicov, J.M. Macak, R. Hahn, P. Schmuki, Self-organized, free-standing TiO_2 nanotube membrane for flow-through photocatalytic applications, Nano Lett. 7 (2007) 1286–1289, http://dx.doi.org/10.1021/nl070264k.
[14] S.P. Albu, A. Ghicov, S. Aldabergenova, P. Drechsel, D. LeClere, G.E. Thompson, J.M. Macak, P. Schmuki, Formation of double-walled TiO_2 nanotubes and robust anatase membranes, Adv. Mater. 20 (2008) 4135–4139, http://dx.doi.org/10.1002/adma.200801189.

[15] R. Kupcik, P. Rehulka, Z. Bilkova, H. Sopha, J.M. Macak, New interface for purification of proteins: one-dimensional TiO_2 nanotubes decorated by Fe_3O_4 nanoparticles, ACS Appl. Mater. Interfaces 9 (2017) 28233–28242, http://dx.doi.org/10.1021/acsami.7b08445.

[16] J.M. Macak, B.G. Gong, M. Hueppe, P. Schmuki, Filling of TiO_2 nanotubes by self-doping and electrodeposition, Adv. Mater. 19 (2007) 3027–3031, http://dx.doi.org/10.1002/adma.200602549.

[17] J.M. Macak, C. Zollfrank, B.J. Rodriguez, H. Tsuchiya, M. Alexe, P. Greil, P. Schmuki, Ordered ferroelectric lead titanate nanocellular structure by conversion of anodic TiO_2 nanotubes, Adv. Mater. 21 (2009) 3121–3125, http://dx.doi.org/10.1002/adma.200900587.

[18] D. Fang, K. Huang, S. Liu, D. Qin, High density copper nanowire arrays deposition inside ordered titania pores by electrodeposition, Electrochem. Commun. 11 (2009) 901–904, http://dx.doi.org/10.1016/j.elecom.2009.02.023.

[19] L. Assaud, V. Heresanu, M. Hanbücken, L. Santinacci, Fabrication of p/n heterojunctions by electrochemical deposition of Cu_2O onto TiO_2 nanotubes, C.R. Chem. 16 (2013) 89–95, http://dx.doi.org/10.1016/j.crci.2012.11.004.

[20] W.-T. Sun, Y. Yu, H.-Y. Pan, X.-F. Gao, Q. Chen, L.-M. Peng, CdS quantum dots sensitized TiO_2 nanotube-array photoelectrodes, J. Am. Chem. Soc. 130 (2008) 1124–1125, http://dx.doi.org/10.1021/ja0777741.

[21] D.R. Baker, P.V. Kamat, Photosensitization of TiO_2 nanostructures with CdS quantum dots: particulate versus tubular support architectures, Adv. Funct. Mater. 19 (2009) 805–811, http://dx.doi.org/10.1002/adfm.200801173.

[22] Q. Wang, J. Qiao, S. Gao, Fabrication of $Zn_xIn_{1-x}S$ quantum dot-sensitized TiO_2 nanotube arrays and their photoelectrochemical properties, Mater. Lett. 131 (2014) 354–357, http://dx.doi.org/10.1016/j.matlet.2014.05.142.

[23] J.M. Macak, T. Kohoutek, L. Wang, R. Beranek, Fast and robust infiltration of functional material inside titania nanotube layers: case study of a chalcogenide glass sensitizer, Nanoscale 5 (2013) 9541, http://dx.doi.org/10.1039/c3nr03014h.

[24] S.H. Ju, S. Han, J.S. Kim, The growth and morphology of copper phthalocyanine on TiO_2 nanotube arrays, J. Ind. Eng. Chem. 19 (2013) 272–278, http://dx.doi.org/10.1016/j.jiec.2012.08.011.

[25] J.E. Yoo, K. Lee, M. Altomare, E. Selli, P. Schmuki, Self-organized arrays of single-metal catalyst particles in TiO_2 cavities: a highly efficient photocatalytic system, Angew. Chem. Int. Ed. 52 (2013) 7514–7517, http://dx.doi.org/10.1002/anie.201302525.

[26] N.T. Nguyen, J. Yoo, M. Altomare, P. Schmuki, "Suspended" Pt nanoparticles over TiO_2 nanotubes for enhanced photocatalytic H_2 evolution, Chem. Commun. 50 (2014) 9653–9656, http://dx.doi.org/10.1039/C4CC04087B.

[27] J. Yoo, K. Lee, P. Schmuki, Templating using self-aligned TiO_2 nanotube stumps: highly ordered metal and polymer bumped arrays, ChemElectroChem 1 (2014) 64–66, http://dx.doi.org/10.1002/celc.201300133.

[28] S.M. George, Atomic layer deposition: an overview, Chem. Rev. 110 (2010) 111–131, http://dx.doi.org/10.1021/cr900056b.

[29] C. Detavernier, J. Dendooven, S. Pulinthanathu Sree, K.F. Ludwig, J.A. Martens, Tailoring nanoporous materials by atomic layer deposition, Chem. Soc. Rev. 40 (2011) 5242, http://dx.doi.org/10.1039/c1cs15091j.

[30] D.H. Kim, M.D. Losego, Q. Peng, G.N. Parsons, Atomic layer deposition for sensitized solar cells: recent progress and prospects, Adv. Mater. Interfaces 3 (2016) 1600354, http://dx.doi.org/10.1002/admi.201600354.

[31] J.A. van Delft, D. Garcia-Alonso, W.M.M. Kessels, Atomic layer deposition for photovoltaics: applications and prospects for solar cell manufacturing, Semicond. Sci. Technol. 27 (2012) 074002, http://dx.doi.org/10.1088/0268-1242/27/7/074002.

[32] W. Niu, X. Li, S.K. Karuturi, D.W. Fam, H. Fan, S. Shrestha, L.H. Wong, A.I.Y. Tok, Applications of atomic layer deposition in solar cells, Nanotechnology 26 (2015) 064001, http://dx.doi.org/10.1088/0957-4484/26/6/064001.

[33] T. Wang, Z. Luo, C. Li, J. Gong, Controllable fabrication of nanostructured materials for photoelectrochemical water splitting via atomic layer deposition, Chem. Soc. Rev. 43 (2014) 7469–7484, http://dx.doi.org/10.1039/C3CS60370A.

[34] C. Marichy, M. Bechelany, N. Pinna, Atomic layer deposition of nanostructured materials for energy and environmental applications, Adv. Mater. 24 (2012) 1017–1032, http://dx.doi.org/10.1002/adma.201104129.

[35] B. Ahmed, C. Xia, H.N. Alshareef, Electrode surface engineering by atomic layer deposition: a promising pathway toward better energy storage, Nano Today 11 (2016) 250–271, http://dx.doi.org/10.1016/j.nantod.2016.04.004.

[36] C. Bae, H. Shin, K. Nielsch, Surface modification and fabrication of 3D nanostructures by atomic layer deposition, MRS Bull. 36 (2011) 887–897, http://dx.doi.org/10.1557/mrs.2011.264.

[37] F.-X. Xiao, J. Miao, H.B. Tao, S.-F. Hung, H.-Y. Wang, H. Bin Yang, J. Chen, R. Chen, B. Liu, One-dimensional hybrid nanostructures for heterogeneous photocatalysis and photoelectrocatalysis, Small 11 (2015) 2115–2131, http://dx.doi.org/10.1002/smll.201402420.

[38] C. Guan, J. Wang, Recent development of advanced electrode materials by atomic layer deposition for electrochemical energy storage, Adv. Sci. 3 (2016) 1500405, http://dx.doi.org/10.1002/advs.201500405.

[39] A.F. Palmstrom, P.K. Santra, S.F. Bent, Atomic layer deposition in nanostructured photovoltaics: tuning optical, electronic and surface properties, Nanoscale 7 (2015) 12266–12283, http://dx.doi.org/10.1039/C5NR02080H.

[40] X. Meng, X. Wang, D. Geng, C. Ozgit-Akgun, N. Schneider, J.W. Elam, Atomic layer deposition for nanomaterials synthesis and functionalization in energy technology, Mater. Horiz. 4 (2017) 133–154, http://dx.doi.org/10.1039/C6MH00521G.

[41] F. Keller, M.S. Hunter, D.L. Robinson, Structural features of oxide coatings on aluminum, J. Electrochem. Soc. 100 (1953) 411, http://dx.doi.org/10.1149/1.2781142.

[42] G.E. Thompson, R.C. Furneaux, G.C. Wood, J.A. Richardson, J.S. Goode, Nucleation and growth of porous anodic films on aluminium, Nature 272 (1978) 433–435, http://dx.doi.org/10.1038/272433a0.

[43] A.M. Md Jani, D. Losic, N.H. Voelcker, Nanoporous anodic aluminium oxide: advances in surface engineering and emerging applications, Prog. Mater. Sci. 58 (2013) 636–704, http://dx.doi.org/10.1016/j.pmatsci.2013.01.002.

[44] S.M. George, O. Sneh, A.C. Dillon, M.L. Wise, A.W. Ott, L.A. Okada, J.D. Way, Atomic layer controlled deposition of SiO_2 and Al_2O_3 using ABAB. . . binary reaction sequence chemistry, Appl. Surf. Sci. 82–83 (1994) 460–467, http://dx.doi.org/10.1016/0169-4332(94)90259-3.

[45] A.C.C. Dillon, A.W. Ott, J.D.D. Way, S.M. George, Surface chemistry of Al_2O_3 deposition using $Al(CH_3)_3$ and H_2O in a binary reaction sequence, Surf. Sci. 322 (1995) 230–242, http://dx.doi.org/10.1016/0039-6028(95)90033-0.

[46] A.W. Ott, K.C. McCarley, J.W. Klaus, J.D. Way, S.M. George, Atomic layer controlled deposition of Al_2O_3 films using binary reaction sequence chemistry, Appl. Surf. Sci. 107 (1996) 128–136, http://dx.doi.org/10.1016/S0169-4332(96)00503-X.

[47] A.W. Ott, J.W. Klaus, J.M. Johnson, S.M. George, K.C. McCarley, J.D. Way, Modification of porous alumina membranes using Al_2O_3 atomic layer controlled deposition, Chem. Mater. 9 (1997) 707–714, http://dx.doi.org/10.1021/cm960377x.

[48] B.S. Berland, I.P. Gartland, A.W. Ott, S.M. George, In situ monitoring of atomic layer controlled pore reduction in alumina tubular membranes using sequential surface reactions, Chem. Mater. 10 (1998) 3941–3950, http://dx.doi.org/10.1021/cm980384g.

[49] M. a Cameron, I.P. Gartland, J. a Smith, S.F. Diaz, S.M. George, Atomic layer deposition of SiO_2 and TiO_2 in alumina tubular membranes: pore reduction and effect of surface species on gas transport, Langmuir 16 (2000) 7435–7444, http://dx.doi.org/10.1021/la9916981.

[50] J.W. Elam, D. Routkevitch, P.P. Mardilovich, S.M. George, Conformal coating on ultrahigh-aspect-ratio nanopores of anodic alumina by atomic layer deposition, Chem. Mater. 15 (2003) 3507–3517, http://dx.doi.org/10.1021/cm0303080.

[51] A. Johansson, T. Törndahl, L.M. Ottosson, M. Boman, J.-O. Carlsson, Copper nanoparticles deposited inside the pores of anodized aluminium oxide using atomic layer deposition, Mater. Sci. Eng. C 23 (2003) 823–826, http://dx.doi.org/10.1016/j.msec.2003.09.139.

[52] J.W. Elam, A. Zinovev, C.Y. Han, H.H. Wang, U. Welp, J.N. Hryn, M.J. Pellin, Atomic layer deposition of palladium films on Al_2O_3 surfaces, Thin Solid Films 515 (2006) 1664–1673, http://dx.doi.org/10.1016/j.tsf.2006.05.049.

[53] M. Daub, M. Knez, U. Goesele, K. Nielsch, Ferromagnetic nanotubes by atomic layer deposition in anodic alumina membranes, J. Appl. Phys. 101 (2007) 09J111, http://dx.doi.org/10.1063/1.2712057.

[54] K. Nielsch, J. Bachmann, M. Daub, J. Jing, M. Knez, U. Gösele, S. Barth, S. Mathur, J. Escrig, D. Altbir, Ferromagnetic nanostructures by atomic layer deposition: from thin films towards core–shell nanotubes, ECS Trans. (2007) 139–148, http://dx.doi.org/10.1149/1.2779078.

[55] W.-H. Kim, S.-J. Park, J.-Y. Son, H. Kim, Ru nanostructure fabrication using an anodic aluminum oxide nanotemplate and highly conformal Ru atomic layer deposition, Nanotechnology 19 (2008) 045302, http://dx.doi.org/10.1088/0957-4484/19/04/045302.

[56] D.J. Comstock, S.T. Christensen, J.W. Elam, M.J. Pellin, M.C. Hersam, Tuning the composition and nanostructure of Pt/Ir films via anodized aluminum oxide templated atomic layer deposition, Adv. Funct. Mater. 20 (2010) 3099–3105, http://dx.doi.org/10.1002/adfm.201000389.

[57] Y.-C. Liang, C.-C. Wang, C.-C. Kei, Y.-C. Hsueh, W.-H. Cho, T.-P. Perng, Photocatalysis of Ag-loaded TiO_2 nanotube arrays formed by atomic layer deposition, J. Phys. Chem. C 115 (2011) 9498–9502, http://dx.doi.org/10.1021/jp202111p.

[58] A. Vaish, S. Krueger, M. Dimitriou, C. Majkrzak, D.J. Vanderah, L. Chen, K. Gawrisch, Enhancing the platinum atomic layer deposition infiltration depth inside anodic alumina nanoporous membrane, J. Vac. Sci. Technol. A: Vac. Surf. Film 33 (2015) 01A148, http://dx.doi.org/10.1116/1.4904398.

[59] V. Pore, M. Ritala, M. Leskelä, Atomic layer deposition of titanium disulfide thin films, Chem. Vap. Deposition 13 (2007) 163–168, http://dx.doi.org/10.1002/cvde.200606530.

[60] J. Yoon, S. Kim, K. No, Highly ordered and well aligned TiN nanotube arrays fabricated via template-assisted atomic layer deposition, Mater. Lett. 87 (2012) 124–126, http://dx.doi.org/10.1016/j.matlet.2012.07.081.

[61] P. Chen, T. Mitsui, D.B. Farmer, J. Golovchenko, R.G. Gordon, D. Branton, Atomic layer deposition to fine-tune the surface properties and diameters of fabricated nanopores, Nano Lett. 4 (2004) 1333–1337, http://dx.doi.org/10.1021/nl0494001.

[62] G. Xiong, J.W. Elam, H. Feng, C.Y. Han, H.-H. Wang, L.E. Iton, L.a. Curtiss, M.J. Pellin, M. Kung, H. Kung, P.C. Stair, Effect of atomic layer deposition coatings on the surface structure of anodic aluminum oxide membranes, J. Phys. Chem. B 109 (2005) 14059–14063, http://dx.doi.org/10.1021/jp0503415.

[63] V. Vega, L. Gelde, A.S. González, V.M. Prida, B. Hernando, J. Benavente, Diffusive transport through surface functionalized nanoporous alumina membranes by atomic layer deposition of metal oxides, J. Ind. Eng. Chem. 52 (2017) 66–72, http://dx.doi.org/10.1016/j.jiec.2017.03.025.

[64] M. Kemell, V. Pore, J. Tupala, M. Ritala, M. Leskelä, Atomic layer deposition of nanostructured TiO_2 photocatalysts via template approach, Chem. Mater. 19 (2007) 1816–1820, http://dx.doi.org/10.1021/cm062576e.

[65] C. Bae, Y. Yoon, H. Yoo, D. Han, J. Cho, B.H. Lee, M.M. Sung, M. Lee, J. Kim, H. Shin, Controlled fabrication of multiwall anatase TiO_2 nanotubular architectures, Chem. Mater. 21 (2009) 2574–2576, http://dx.doi.org/10.1021/cm803112p.

[66] M. Kemell, E. Härkönen, V. Pore, M. Ritala, M. Leskelä, Ta_2O_5- and TiO_2-based nanostructures made by atomic layer deposition, Nanotechnology 21 (2010) 035301, http://dx.doi.org/10.1088/0957-4484/21/3/035301.

[67] S.K. Panda, Y. Yoon, H.S. Jung, W.-S. Yoon, H. Shin, Nanoscale size effect of titania (anatase) nanotubes with uniform wall thickness as high performance anode for lithium-ion secondary battery, J. Power Sources 204 (2012) 162–167, http://dx.doi.org/10.1016/j.jpowsour.2011.12.048.

[68] J. Lee, D.H. Kim, S.-H. Hong, J.Y. Jho, A hydrogen gas sensor employing vertically aligned TiO_2 nanotube arrays prepared by template-assisted method, Sens. Actuators B: Chem. 160 (2011) 1494–1498, http://dx.doi.org/10.1016/j.snb.2011.08.001.

[69] J. Bachmann, J. Jing, M. Knez, S. Barth, H. Shen, S. Mathur, U. Gösele, K. Nielsch, U. G?sele, K. Nielsch, Ordered iron oxide nanotube arrays of controlled geometry and tunable magnetism by atomic layer deposition, J. Am. Chem. Soc. 129 (2007) 9554–9555, http://dx.doi.org/10.1021/ja072465w.

[70] J. Bachmann, R. Zierold, Y.T. Chong, R. Hauert, C. Sturm, R. Schmidt-Grund, B. Rheinländer, M. Grundmann, U. Gösele, K. Nielsch, A practical, self-catalytic, atomic layer deposition of silicon dioxide, Angew. Chem. Int. Ed. 47 (2008) 6177–6179, http://dx.doi.org/10.1002/anie.200800245.

[71] L. Velleman, G. Triani, P.J. Evans, J.G. Shapter, D. Losic, Structural and chemical modification of porous alumina membranes, Microporous Mesoporous Mater. 126 (2009) 87–94, http://dx.doi.org/10.1016/j.micromeso.2009.05.024.

[72] V. Romero, V. Vega, J. García, R. Zierold, K. Nielsch, V.M. Prida, B. Hernando, J. Benavente, Changes in morphology and ionic transport induced by ALD SiO_2 coating of nanoporous alumina membranes, ACS Appl. Mater. Interfaces. 5 (2013) 3556–3564, http://dx.doi.org/10.1021/am400300r.

[73] C. Bae, H. Kim, Y. Yang, H. Yoo, J.M. Montero Moreno, J. Bachmann, K. Nielsch, H. Shin, Rapid, conformal gas-phase formation of silica (SiO_2) nanotubes from water condensates, Nanoscale 5 (2013) 5825, http://dx.doi.org/10.1039/c3nr00906h.

[74] A.B.F. Martinson, J.W. Elam, J.T. Hupp, M.J. Pellin, ZnO nanotube based dye-sensitized solar cells, Nano Lett. 7 (2007) 2183–2187, http://dx.doi.org/10.1021/nl070160+.

[75] C.-J. Yang, S.-M. Wang, S.-W. Liang, Y.-H. Chang, C. Chen, J.-M. Shieh, Low-temperature growth of ZnO nanorods in anodic aluminum oxide on Si substrate by atomic layer deposition, Appl. Phys. Lett. 90 (2007) 033104, http://dx.doi.org/10.1063/1.2431786.

[76] Y.-H. Chang, S.-M. Wang, C.-M. Liu, C. Chen, Fabrication and characteristics of self-aligned ZnO nanotube and nanorod arrays on Si substrates by atomic layer deposition, J. Electrochem. Soc. 157 (2010) K236, http://dx.doi.org/10.1149/1.3489953.

[77] R.J. Narayan, S.P. Adiga, M.J. Pellin, L.A. Curtiss, S. Stafslien, B. Chisholm, N.A. Monteiro-Riviere, R.L. Brigmon, J.W. Elam, Atomic layer deposition of nanoporous biomaterials, Mater. Today 13 (2010) 60–64, http://dx.doi.org/10.1016/S1369-7021(10)70035-3.

[78] S.A. Skoog, M.R. Bayati, P.E. Petrochenko, S. Stafslien, J. Daniels, N. Cilz, D.J. Comstock, J.W. Elam, R.J. Narayan, Antibacterial activity of zinc oxide-coated nanoporous alumina, Mater. Sci. Eng. B 177 (2012) 992–998, http://dx.doi.org/10.1016/j.mseb.2012.04.024.

[79] J.W. Elam, D.A. Baker, A.J. Hryn, A.B.F. Martinson, M.J. Pellin, J.T. Hupp, Atomic layer deposition of tin oxide films using tetrakis(dimethylamino) tin, J. Vac. Sci. Technol. A: Vac. Surf. Film 26 (2008) 244–252, http://dx.doi.org/10.1116/1.2835087.

[80] M. Diskus, O. Nilsen, H. Fjellvåg, Thin films of cobalt oxide deposited on high aspect ratio supports by atomic layer deposition, Chem. Vap. Deposition 17 (2011) 135–140, http://dx.doi.org/10.1002/cvde.201006891.

[81] Y. Wu, L. Assaud, C. Kryschi, B. Capon, C. Detavernier, L. Santinacci, J. Bachmann, Antimony sulfide as a light absorber in highly ordered, coaxial nanocylindrical arrays: preparation and integration into a photovoltaic device, J. Mater. Chem. A 3 (2015) 5971–5981, http://dx.doi.org/10.1039/C5TA00111K.

[82] M.K.S. Barr, L. Assaud, Y. Wu, C. Laffon, P. Parent, J. Bachmann, L. Santinacci, Engineering a three-dimensional, photoelectrochemically active p-NiO/i-Sb_2S_3 junction by atomic layer deposition, Electrochim. Acta 179 (2015) 504–511, http://dx.doi.org/10.1016/j.electacta.2015.07.016.

[83] K. Pitzschel, J.M.M. Moreno, J. Escrig, O. Albrecht, K. Nielsch, J. Bachmann, Controlled introduction of diameter modulations in arrayed magnetic iron oxide nanotubes, ACS Nano 3 (2009) 3463–3468, http://dx.doi.org/10.1021/nn900909q.

[84] R. Zierold, Z. Wu, J. Biskupek, U. Kaiser, J. Bachmann, C.E. Krill, K. Nielsch, Magnetic, multilayered nanotubes of low aspect ratios for liquid suspensions, Adv. Funct. Mater. 21 (2011) 226–232, http://dx.doi.org/10.1002/adfm.201001395.

[85] K. Pitzschel, J. Bachmann, J.M. Montero-Moreno, J. Escrig, D. Görlitz, K. Nielsch, Reversal modes and magnetostatic interactions in $Fe_3O_4/ZrO_2/Fe_3O_4$ multilayer nanotubes, Nanotechnology 23 (2012) 495718, http://dx.doi.org/10.1088/0957-4484/23/49/495718.

[86] G. Armelles, A. Cebollada, A. García-Martín, J.M. Montero-Moreno, M. Waleczek, K. Nielsch, Magneto-optical properties of core–shell magneto-plasmonic Au–$Co_xFe_{3-x}O_4$ nanowires, Langmuir 28 (2012) 9127–9130, http://dx.doi.org/10.1021/la300431a.

[87] R.J. Narayan, S.P. Adiga, M.J. Pellin, L. a Curtiss, A.J. Hryn, S. Stafslien, B. Chisholm, C.-C. Shih, C.-M. Shih, S.-J. Lin, Y.-Y. Su, C. Jin, J. Zhang, N. a Monteiro-Riviere, J.W. Elam, Atomic layer deposition-based functionalization of materials for medical and environmental health applications, Philos. Trans. R. Soc. A: Math. Phys. Eng. Sci. 368 (2010) 2033–2064, http://dx.doi.org/10.1098/rsta.2010.0011.

[88] S.J. Ku, G.C. Jo, C.H. Bak, S.M. Kim, Y.R. Shin, K.H. Kim, S.H. Kwon, J.-B. Kim, Highly ordered freestanding titanium oxide nanotube arrays using Si-containing block copolymer lithography and atomic layer deposition, Nanotechnology 24 (2013) 085301, http://dx.doi.org/10.1088/0957-4484/24/8/085301.

[89] C. Guerra-Nuñez, Y. Zhang, M. Li, V. Chawla, R. Erni, J. Michler, H.G. Park, I. Utke, Morphology and crystallinity control of ultrathin TiO_2 layers deposited on carbon nanotubes by temperature-step atomic layer deposition, Nanoscale 7 (2015) 10622–10633, http://dx.doi.org/10.1039/C5NR02106E.

[90] X.L. Li, C. Li, Y. Zhang, D.P. Chu, W.I. Milne, H.J. Fan, Atomic layer deposition of ZnO on multi-walled carbon nanotubes and its use for synthesis of CNT-ZnO heterostructures, Nanoscale Res. Lett. 5 (2010) 1836–1840, http://dx.doi.org/10.1007/s11671-010-9721-z.

[91] R. Pietruszka, B.S. Witkowski, G. Luka, L. Wachnicki, S. Gieraltowska, K. Kopalko, E. Zielony, P. Bieganski, E. Placzek-Popko, M. Godlewski, Photovoltaic properties of ZnO nanorods/p-type Si heterojunction structures, Beilstein J. Nanotechnol. 5 (2014) 173–179, http://dx.doi.org/10.3762/bjnano.5.17.

[92] M.E. Edley, S. Li, G.W. Guglietta, H. Majidi, J.B. Baxter, Ultrafast charge carrier dynamics in extremely thin absorber (ETA) solar cells consisting of CdSe-coated ZnO nanowires, J. Phys. Chem. C 120 (2016) 19504–19512, http://dx.doi.org/10.1021/acs.jpcc.6b03974.

[93] A. Kargar, K. Sun, Y. Jing, C. Choi, H. Jeong, G.Y. Jung, S. Jin, D. Wang, 3D branched nanowire photoelectrochemical electrodes for efficient solar water splitting, ACS Nano 7 (2013) 9407–9415, http://dx.doi.org/10.1021/nn404170y.

[94] K. Yuan, Q. Cao, X. Li, H.Y. Chen, Y. Deng, Y.Y. Wang, W. Luo, H.L. Lu, D.W. Zhang, Synthesis of WO_3@$ZnWO_4$@ZnO–ZnO hierarchical nanocactus arrays for efficient photoelectrochemical water splitting, Nano Energy 41 (2017) 543–551, http://dx.doi.org/10.1016/j.nanoen.2017.09.053.

[95] R.G. Gordon, D. Hausmann, E. Kim, J. Shepard, A kinetic model for step coverage by atomic layer deposition in narrow holes or trenches, Chem. Vap. Deposition 9 (2003) 73–78, http://dx.doi.org/10.1002/cvde.200390005.

[96] J.-Y. Kim, J.-H. Ahn, S.-W. Kang, J.-H. Kim, Step coverage modeling of thin films in atomic layer deposition, J. Appl. Phys. 101 (2007) 073502, http://dx.doi.org/10.1063/1.2714685.

[97] J. Dendooven, D. Deduytsche, J. Musschoot, R.L. Vanmeirhaeghe, C. Detavernier, Modeling the conformality of atomic layer deposition: the effect of sticking probability, J. Electrochem. Soc. 156 (2009) P63, http://dx.doi.org/10.1149/1.3072694.

[98] M. Rose, J.W. Bartha, Method to determine the sticking coefficient of precursor molecules in atomic layer deposition, Appl. Surf. Sci. 255 (2009) 6620–6623, http://dx.doi.org/10.1016/j.apsusc.2009.02.055.

[99] R.A. Adomaitis, Development of a multiscale model for an atomic layer deposition process, J. Cryst. Growth 312 (2010) 1449–1452, http://dx.doi.org/10.1016/j.jcrysgro.2009.12.041.

[100] H.C.M. Knoops, E. Langereis, M.C.M. van de Sanden, W.M.M. Kessels, Conformality of plasma-assisted ALD: physical processes and modeling, J. Electrochem. Soc. 157 (2010) G241, http://dx.doi.org/10.1149/1.3491381.

[101] A. Yanguas-Gil, J.W. Elam, A Markov chain approach to simulate atomic layer deposition chemistry and transport inside nanostructured substrates, Theor. Chem. Acc. 133 (2014) 1–13, http://dx.doi.org/10.1007/s00214-014-1465-x.

[102] V. Cremers, F. Geenen, C. Detavernier, J. Dendooven, Monte Carlo simulations of atomic layer deposition on 3D large surface area structures: Required precursor exposure for pillar- versus hole-type structures, J. Vac. Sci. Technol. A: Vac. Surf. Film 35 (2017) 01B115, http://dx.doi.org/10.1116/1.4968201.

[103] M.C. Schwille, J. Barth, T. Schössler, F. Schön, J.W. Bartha, M. Oettel, Simulation approach of atomic layer deposition in large 3D structures, Modell. Simul. Mater. Sci. Eng. 25 (2017) 035008, http://dx.doi.org/10.1088/1361-651X/aa5f9d.

[104] M.K. Gobbert, V. Prasad, T.S. Cale, Modeling and simulation of atomic layer deposition at the feature scale, J. Vac. Sci. Technol. B: Microelectron. Nanom. Struct. 20 (2002) 1031, http://dx.doi.org/10.1116/1.1481754.

[105] A. Yanguas-Gil, J.W. Elam, Simple model for atomic layer deposition precursor reaction and transport in a viscous-flow tubular reactor, J. Vac. Sci. Technol. A: Vac. Surf. Film 30 (2012) 01A159, http://dx.doi.org/10.1116/1.3670396.

[106] A. Yanguas-Gil, J.W. Elam, Self-limited reaction–diffusion in nanostructured substrates: surface coverage dynamics and analytic approximations to ALD saturation times, Chem. Vap. Deposition 18 (2012) 46–52, http://dx.doi.org/10.1002/cvde.201106938.

[107] N. Yazdani, V. Chawla, E. Edwards, V. Wood, H.G. Park, I. Utke, Modeling and optimization of atomic layer deposition processes on vertically aligned carbon nanotubes, Beilstein J. Nanotechnol. 5 (2014) 234–244, http://dx.doi.org/10.3762/bjnano.5.25.

[108] T. Keuter, N.H. Menzler, G. Mauer, F. Vondahlen, R. Vaßen, H.P. Buchkremer, Modeling precursor diffusion and reaction of atomic layer deposition in porous structures, J. Vac. Sci. Technol. A: Vac. Surf. Film 33 (2015) 01A104, http://dx.doi.org/10.1116/1.4892385.
[109] R.L. Puurunen, Growth per cycle in atomic layer deposition: a theoretical model, Chem. Vap. Deposition 9 (2003) 249–257, http://dx.doi.org/10.1002/cvde.200306265.
[110] A. Yanguas-Gil, N. Kumar, Y. Yang, J.R. Abelson, Highly conformal film growth by chemical vapor deposition. II. Conformality enhancement through growth inhibition, J. Vac. Sci. Technol. A: Vac. Surf. Film 27 (2009) 1244–1248, http://dx.doi.org/10.1116/1.3207746.
[111] H.C.M. Knoops, J.W. Elam, J.A. Libera, W.M.M. Kessels, Surface loss in ozone-based atomic layer deposition processes, Chem. Mater. 23 (2011) 2381–2387, http://dx.doi.org/10.1021/cm2001144.
[112] J. Dendooven, D. Deduytsche, J. Musschoot, R.L. Vanmeirhaeghe, C. Detavernier, Conformality of Al_2O_3 and AlN deposited by plasma-enhanced atomic layer deposition, J. Electrochem. Soc. 157 (2010) G111, http://dx.doi.org/10.1149/1.3301664.
[113] J.M. Macak, H. Tsuchiya, L. Taveira, S. Aldabergerova, P. Schmuki, Smooth anodic TiO_2 nanotubes, Angew. Chem. Int. Ed. 44 (2005) 7463–7465, http://dx.doi.org/10.1002/anie.200502781.
[114] J.M. Macak, P. Schmuki, Anodic growth of self-organized anodic TiO_2 nanotubes in viscous electrolytes, Electrochim. Acta 52 (2006) 1258–1264, http://dx.doi.org/10.1016/j.electacta.2006.07.021.
[115] S.K. Sarkar, J.Y. Kim, D.N. Goldstein, N.R. Neale, K. Zhu, C.M. Elliott, A.J. Frank, S.M. George, In_2S_3 atomic layer deposition and its application as a sensitizer on TiO_2 nanotube arrays for solar energy conversion, J. Phys. Chem. C 114 (2010) 8032–8039, http://dx.doi.org/10.1021/jp9086943.
[116] J. Tupala, M. Kemell, E. Härkönen, M. Ritala, M. Leskelä, Preparation of regularly structured nanotubular TiO_2 thin films on ITO and their modification with thin ALD-grown layers, Nanotechnology 23 (2012) 125707, http://dx.doi.org/10.1088/0957-4484/23/12/125707.
[117] J.M. Macak, J. Prikryl, H. Sopha, L. Strizik, Antireflection In_2O_3 coatings of self-organized TiO_2 nanotube layers prepared by atomic layer deposition, Phys. Status Solidi Rapid Res. Lett. 9 (2015) 516–520, http://dx.doi.org/10.1002/pssr201510245.
[118] R. Zazpe, M. Knaut, H. Sopha, L. Hromadko, M. Albert, J. Prikryl, V. Gärtnerová, J.W. Bartha, J.M. Macak, Atomic layer deposition for coating of high aspect ratio TiO_2 nanotube layers, Langmuir 32 (2016) 10551–10558, http://dx.doi.org/10.1021/acs.langmuir.6b03119.
[119] A. Hagfeldt, G. Boschloo, L. Sun, L. Kloo, H. Pettersson, Dye-sensitized solar cells, Chem. Rev. 110 (2010) 6595–6663, http://dx.doi.org/10.1021/cr900356p.
[120] T. Ohno, F. Tanigawa, K. Fujihara, S. Izumi, M. Matsumura, Photocatalytic oxidation of water by visible light using ruthenium-doped titanium dioxide powder, J. Photochem. Photobiol. A: Chem. 127 (1999) 107–110, http://dx.doi.org/10.1016/S1010-6030(99)00128-8.
[121] R. Asahi, T. Morikawa, T. Ohwaki, K. Aoki, Y. Taga, Visible-light photocatalysis in nitrogen-doped titanium oxides, Science (80-) 293 (2001) 269–271, http://dx.doi.org/10.1126/science.1061051.
[122] C. Burda, Y. Lou, X. Chen, A.C.S. Samia, J. Stout, J.L. Gole, Enhanced nitrogen doping in TiO_2 nanoparticles, Nano Lett. 3 (2003) 1049–1051, http://dx.doi.org/10.1021/nl034332o.
[123] M. Anpo, S. Dohshi, M. Kitano, Y. Hu, M. Takeuchi, M. Matsuoka, The preparation and characterization of highly efficient titanium oxide-based photofunctional materials, Annu. Rev. Mater. Res. 35 (2005) 1–27, http://dx.doi.org/10.1146/annurev.matsci.35.100303.121340.
[124] S. Sakthivel, H. Kisch, Daylight photocatalysis by carbon-modified titanium dioxide, Angew. Chem. Int. Ed. 42 (2003) 4908–4911, http://dx.doi.org/10.1002/anie.200351577.
[125] R. Zazpe, H. Sopha, J. Prikryl, M. Krbal, J. Mistrik, F. Dvorak, L. Hromadko, J.M. Macak, A 1D conical nanotubular TiO_2/CdS heterostructure with superior photon-to-electron conversion, Nanoscale 10 (2018) 16601–16612, http://dx.doi.org/10.1039/C8NR02418A.
[126] E. Rabinovich, G. Hodes, Effective bandgap lowering of CdS deposited by successive ionic layer adsorption and reaction, J. Phys. Chem. C 117 (2013) 1611–1620, http://dx.doi.org/10.1021/jp3105453.
[127] M.V. Malashchonak, A.V. Mazanik, O.V. Korolik, E.A. Streltsov, A.I. Kulak, Influence of wide band gap oxide substrates on the photoelectrochemical properties and structural disorder of CdS nanoparticles grown by the successive ionic layer adsorption and reaction (SILAR) method, Beilstein J. Nanotechnol. 6 (2015) 2252–2262, http://dx.doi.org/10.3762/bjnano.6.231.
[128] B. Huang, W. Yang, Y. Wen, B. Shan, R. Chen, Co_3O_4-modified TiO_2 nanotube arrays via atomic layer deposition for improved visible-light photoelectrochemical performance, ACS Appl. Mater. Interfaces 7 (2015) 422–431, http://dx.doi.org/10.1021/am506392y.
[129] H.K. Jun, M.A. Careem, A.K. Arof, Quantum dot-sensitized solar cells-perspective and recent developments: a review of Cd chalcogenide quantum dots as sensitizers, Renew. Sustain. Energy Rev. 22 (2013) 148–167, http://dx.doi.org/10.1016/j.rser.2013.01.030.
[130] Y. Yu, J. Ren, M. Meng, Photocatalytic hydrogen evolution on graphene quantum dots anchored TiO_2 nanotubes-array, Int. J. Hydrogen Energy 38 (2013) 12266–12272, http://dx.doi.org/10.1016/j.ijhydene.2013.07.039.
[131] Y. Zhu, Y. Wang, Z. Chen, L. Qin, L. Yang, L. Zhu, P. Tang, T. Gao, Y. Huang, Z. Sha, G. Tang, Visible light induced photocatalysis on CdS quantum dots decorated TiO_2 nanotube arrays, Appl. Catal. A: Gen. 498 (2015) 159–166, http://dx.doi.org/10.1016/j.apcata.2015.03.035.
[132] Y. Liu, H. Zhou, B. Zhou, J. Li, H. Chen, J. Wang, J. Bai, W. Shangguan, W. Cai, Highly stable CdS-modified short TiO_2 nanotube array electrode for efficient visible-light hydrogen generation, Int. J. Hydrogen Energy 36 (2011) 167–174, http://dx.doi.org/10.1016/j.ijhydene.2010.09.089.
[133] J.R. Jennings, A. Ghicov, L.M. Peter, P. Schmuki, A.B. Walker, Dye-sensitized solar cells based on oriented TiO_2 nanotube arrays: transport, trapping, and transfer of electrons, J. Am. Chem. Soc. 130 (2008) 13364–13372, http://dx.doi.org/10.1021/ja804852z.
[134] M. Krbal, J. Prikryl, R. Zazpe, H. Sopha, J.M. Macak, CdS-coated TiO_2 nanotube layers: downscaling tube diameter towards efficient heterostructured photoelectrochemical conversion, Nanoscale 9 (2017) 7755–7759, http://dx.doi.org/10.1039/C7NR02841E.
[135] S. Ng, M. Krbal, R. Zazpe, J. Prikryl, J. Charvot, F. Dvořák, L. Strizik, S. Slang, H. Sopha, Y. Kosto, V. Matolin, F.K. Yam, F. Bures, J.M. Macak, $MoSe_xO_y$-coated 1D TiO_2 nanotube layers: efficient interface for light-driven applications, Adv. Mater. Interfaces 1701146 (2017) 1701146, http://dx.doi.org/10.1002/admi.201701146.
[136] M. Krbal, J. Prikryl, R. Zazpe, F. Dvorak, F. Bures, J.M. Macak, 2D $MoSe_2$ structures prepared by atomic layer deposition, Phys. Status Solidi Rapid Res. Lett. 1800023 (2018) 4–7, http://dx.doi.org/10.1002/pssr.201800023.
[137] A. Hagfeldt, M. Grätzel, Light-induced redox reactions in nanocrystalline systems, Chem. Rev. 95 (1995) 49–68, http://dx.doi.org/10.1021/cr00033a003.
[138] S. Wendt, P.T. Sprunger, E. Lira, G.K.H. Madsen, Z. Li, J. Hansen, J. Matthiesen, A. Blekinge-Rasmussen, E. Lægsgaard, B. Hammer, F. Besenbacher, The role of interstitial sites in the Ti3d defect state in the band gap of titania, Science (80-) 320 (2008) 1755–1759, http://dx.doi.org/10.1126/science.1159846.
[139] J.-Y. Kim, K.-H. Lee, J. Shin, S.H. Park, J.S. Kang, K.S. Han, M.M. Sung, N. Pinna, Y.-E. Sung, Highly ordered and vertically oriented TiO_2/Al_2O_3 nanotube electrodes for application in dye-sensitized solar cells, Nanotechnology 25 (2014) 504003, http://dx.doi.org/10.1088/0957-4484/25/50/504003.
[140] Q. Gui, Z. Xu, H. Zhang, C. Cheng, X. Zhu, M. Yin, Y. Song, L. Lu, X. Chen, D. Li, Enhanced photoelectrochemical water splitting performance of anodic TiO_2 nanotube arrays by surface passivation, ACS Appl. Mater. Interfaces 6 (2014) 17053–17058, http://dx.doi.org/10.1021/am504662w.
[141] M. Zeng, X. Peng, J. Liao, G. Wang, Y. Li, J. Li, Y. Qin, J. Wilson, A. Song, S. Lin, Enhanced photoelectrochemical performance of quantum dot-sensitized TiO_2 nanotube arrays with Al_2O_3 overcoating by atomic layer deposition, Phys. Chem. Chem. Phys. 18 (2016) 17404–17413, http://dx.doi.org/10.1039/C6CP01299J.
[142] Q. Zhou, J. Zhou, M. Zeng, G. Wang, Y. Chen, S. Lin, Photoelectrochemical performance of quantum dot-sensitized TiO_2 nanotube arrays: a study of surface modification by atomic layer deposition coating, Nanoscale Res. Lett. 12 (2017) 261, http://dx.doi.org/10.1186/s11671-017-2036-6.
[143] J.-S. Jeong, B.-H. Choe, J.-H. Lee, J.-J. Lee, W.-Y. Choi, ZnO-coated TiO_2 nanotube arrays for a photoelectrode in dye-sensitized solar cells, J. Electron. Mater. 43 (2014) 375–380, http://dx.doi.org/10.1007/s11664-013-2908-1.
[144] H. Cai, Q. Yang, Z. Hu, Z. Duan, Q. You, J. Sun, N. Xu, J. Wu, Enhanced photoelectrochemical activity of vertically aligned ZnO-coated TiO_2 nanotubes, Appl. Phys. Lett. 104 (2014) 053114, http://dx.doi.org/10.1063/1.4863852.
[145] H. Cai, Q. You, Z. Hu, Z. Duan, Y. Cui, J. Sun, N. Xu, J. Wu, Fabrication and correlation between photoluminescence and photoelectrochemical properties of vertically aligned ZnO coated TiO_2 nanotube arrays, Sol. Energy Mater. Sol. Cells 123 (2014) 233–238, http://dx.doi.org/10.1016/j.solmat.2014.01.033.
[146] M. Zeng, X. Zeng, X. Peng, Z. Zhu, J. Liao, K. Liu, G. Wang, S. Lin, Improving photoelectrochemical performance on quantum dots co-sensitized TiO_2 nanotube arrays using ZnO energy barrier by atomic layer deposition, Appl. Surf. Sci. 388 (2016) 352–358, http://dx.doi.org/10.1016/j.apsusc.2015.12.169.
[147] H. Cai, P. Liang, Z. Hu, L. Shi, X. Yang, J. Sun, N. Xu, J. Wu, Enhanced photoelectrochemical activity of ZnO-coated TiO_2 nanotubes and its dependence on ZnO coating thickness, Nanoscale Res. Lett. 11 (2016) 1–11, http://dx.doi.org/10.1186/s11671-016-1309-9.
[148] H. Cai, X. Yang, W. Zhang, H. Li, Y. Qiu, N. Xu, J. Wu, J. Sun, Enhanced light absorption and quenched photoluminescence resulting in photoactive poly(3-hexyl-thiophene)-covered ZnO/TiO_2 nanotubes for high light harvesting efficiency, Sol. Energy Mater. Sol. Cells 162 (2017) 47–54, http://dx.doi.org/10.1016/j.solmat.2016.12.040.
[149] H. Sopha, M. Krbal, S. Ng, J. Prikryl, R. Zazpe, F.K. Yam, J.M. Macak, Highly efficient photoelectrochemical and photocatalytic anodic TiO_2 nanotube layers with additional TiO_2 coating, Appl. Mater. Today 9 (2017) 104–110, http://dx.doi.org/10.1016/j.apmt.2017.06.002.
[150] K. Yu, X. Lin, G. Lu, Z. Wen, C. Yuan, J. Chen, Optimized CdS quantum dot-sensitized solar cell performance through atomic layer deposition of ultrathin TiO_2 coating, RSC Adv. 2 (2012) 7843, http://dx.doi.org/10.1039/c2ra20979a.
[151] C.Y. Jiang, W.L. Koh, M.Y. Leung, S.Y. Chiam, J.S. Wu, J. Zhang, Low temperature processing solid-state dye sensitized solar cells, Appl. Phys. Lett. 100 (2012), http://dx.doi.org/10.1063/1.3693399.
[152] D.H. Kim, M. Woodroof, K. Lee, G.N. Parsons, Atomic layer deposition of high performance ultrathin TiO_2 blocking layers for dye-sensitized solar cells,

ChemSusChem 6 (2013) 1014–1020, http://dx.doi.org/10.1002/cssc.201300067.
[153] L. Kavan, N. Tétreault, T. Moehl, M. Grätzel, Electrochemical characterization of TiO_2 blocking layers for dye-sensitized solar cells, J. Phys. Chem. C 118 (2014) 16408–16418, http://dx.doi.org/10.1021/jp4103614.
[154] J.-H. Yum, T. Moehl, J. Yoon, A.K. Chandiran, F. Kessler, P. Gratia, M. Grätzel, Toward higher photovoltage: effect of blocking layer on cobalt bipyridine pyrazole complexes as redox shuttle for dye-sensitized solar cells, J. Phys. Chem. C 118 (2014) 16799–16805, http://dx.doi.org/10.1021/jp412777.
[155] G. Dingemans, W.M.M. Kessels, Status and prospects of Al_2O_3-based surface passivation schemes for silicon solar cells, J. Vac. Sci. Technol. A: Vac. Surf. Film 30 (2012) 040802, http://dx.doi.org/10.1116/1.4728205.
[156] G. Dingemans, W. Beyer, M.C.M. Van De Sanden, W.M.M. Kessels, Hydrogen induced passivation of Si interfaces by Al_2O_3 films and SiO_2/Al_2O_3 stacks, Appl. Phys. Lett. 97 (2010) 2008–2011, http://dx.doi.org/10.1063/1.3497014.
[157] B. Hoex, J.J.H. Gielis, M.C.M. van de Sanden, W.M.M. Kessels, On the c-Si surface passivation mechanism by the negative-charge-dielectric Al_2O_3, J. Appl. Phys. 104 (2008) 113703, http://dx.doi.org/10.1063/1.3021091.
[158] G. Dingemans, M.C.M. van de Sanden, W.M.M. Kessels, Influence of the deposition temperature on the c-Si surface passivation by Al_2O_3 films synthesized by ALD and PECVD, Electrochem. Solid-State Lett. 13 (2010) H76, http://dx.doi.org/10.1149/1.3276040.
[159] S.J. Roh, R.S. Mane, S.K. Min, W.J. Lee, C.D. Lokhande, S.H. Han, Achievement of 4.51% conversion efficiency using ZnO recombination barrier layer in TiO_2 based dye-sensitized solar cells, Appl. Phys. Lett. 89 (2006) 1–4, http://dx.doi.org/10.1063/1.2410240.
[160] A.K. Chandiran, M. Abdi-Jalebi, M.K. Nazeeruddin, M. Grätzel, Analysis of electron transfer properties of ZnO and TiO_2 photoanodes for dye-sensitized solar cells, ACS Nano 8 (2014) 2261–2268, http://dx.doi.org/10.1021/nn405535j.
[161] Y. Hwang, C. Hahn, B. Liu, P. Yang, Photoelectrochemical properties of TiO_2 nanowire arrays: a study of the dependence on length and atomic layer deposition coating, ACS Nano 6 (2012) 5060–5069, http://dx.doi.org/10.1021/nn300679d.
[162] S.S. Mali, C.S. Shim, H.K. Park, J. Heo, P.S. Patil, C.K. Hong, Ultrathin atomic layer deposited TiO_2 for surface passivation of hydrothermally grown 1D TiO_2 nanorod arrays for efficient solid-state perovskite solar cells, Chem. Mater. 27 (2015) 1541–1551, http://dx.doi.org/10.1021/cm504558g.
[163] S. So, I. Hwang, P. Schmuki, Hierarchical DSSC structures based on "single walled" TiO_2 nanotube arrays reach a back-side illumination solar light conversion efficiency of 8%, Energy Environ. Sci. 8 (2015) 849–854, http://dx.doi.org/10.1039/C4EE03729D.
[164] I. Hwang, S. So, M. Mokhtar, A. Alshehri, S.A. Al-Thabaiti, A. Mazare, P. Schmuki, Single-walled TiO_2 nanotubes: enhanced carrier-transport properties by $TiCl_4$ treatment, Chem. Eur. J. 21 (2015) 9204–9208, http://dx.doi.org/10.1002/chem.201500730.
[165] N.T. Nguyen, I. Hwang, T. Kondo, T. Yanagishita, H. Masuda, P. Schmuki, Optimizing TiO_2 nanotube morphology for enhanced photocatalytic H_2 evolution using single-walled and highly ordered TiO_2 nanotubes decorated with dewetted Au nanoparticles, Electrochem. Commun. 79 (2017) 46–50, http://dx.doi.org/10.1016/j.elecom.2017.04.016.
[166] M. Motola, H. Sopha, M. Krbal, L. Hromádko, G. Plesch, J.M. Macák, Comparison of photoelectrochemical performance of anodic single- and double-walled TiO_2 nanotube layers, Electrochem. Commun. (2018).
[167] J. Schneider, M. Matsuoka, M. Takeuchi, J. Zhang, Y. Horiuchi, M. Anpo, D.W. Bahnemann, Understanding TiO_2 photocatalysis: mechanisms and materials, Chem. Rev. 114 (2014) 9919–9986, http://dx.doi.org/10.1021/cr5001892.
[168] I. Paramasivam, H. Jha, N. Liu, P. Schmuki, A review of photocatalysis using self-organized TiO_2 nanotubes and other ordered oxide nanostructures, Small 8 (2012) 3073–3103, http://dx.doi.org/10.1002/smll.201200564.
[169] J.M. Macak, P.J. Barczuk, H. Tsuchiya, M.Z. Nowakowska, A. Ghicov, M. Chojak, S. Bauer, S. Virtanen, P.J. Kulesza, P. Schmuki, Self-organized nanotubular TiO_2 matrix as support for dispersed Pt/Ru nanoparticles: enhancement of the electrocatalytic oxidation of methanol, Electrochem. Commun. 7 (2005) 1417–1422, http://dx.doi.org/10.1016/j.elecom.2005.09.031.
[170] Y.Y. Song, Z. Da Gao, J.H. Wang, X.H. Xia, R. Lynch, Multistage coloring electrochromic device based on TiO_2 nanotube arrays modified with WO_3 nanoparticles, Adv. Funct. Mater. 21 (2011) 1941–1946, http://dx.doi.org/10.1002/adfm.201002258.
[171] C.W. Lai, S. Sreekantan, Incorporation of WO_3 species into TiO_2 nanotubes via wet impregnation and their water-splitting performance, Electrochim. Acta 87 (2013) 294–302, http://dx.doi.org/10.1016/j.electacta.2012.09.022.
[172] L. Assaud, N. Brazeau, M.K.S. Barr, M. Hanbücken, S. Ntais, E.A. Baranova, L. Santinacci, Atomic layer deposition of Pd nanoparticles on TiO_2 nanotubes for ethanol electrooxidation: synthesis and electrochemical properties, ACS Appl. Mater. Interfaces 7 (2015) 24533–24542, http://dx.doi.org/10.1021/acsami.5b06056.
[173] J. Yoo, R. Zazpe, G. Cha, J. Prikryl, I. Hwang, J.M. Macak, P. Schmuki, Uniform ALD deposition of Pt nanoparticles within 1D anodic TiO_2 nanotubes for photocatalytic H_2 generation, Electrochem. Commun. 86 (2018) 6–11, http://dx.doi.org/10.1016/j.elecom.2017.10.017.
[174] V.C. Anitha, R. Zazpe, M. Krbal, J. Yoo, H. Sopha, J. Prikryl, G. Cha, S. Slang, P. Schmuki, J.M. Macak, Anodic TiO_2 nanotubes decorated by Pt nanoparticles using ALD: an efficient electrocatalyst for methanol oxidation, J. Catal. 365 (2018) 86–93, http://dx.doi.org/10.1016/j.jcat.2018.06.017.
[175] I. Turkevych, S. Kosar, Y. Pihosh, K. Mawatari, T. Kitamori, J. Ye, K. Shimamura, Synergistic effect between TiO_2 and ubiquitous metal oxides on photocatalytic activity of composite nanostructures, Nippon Seramikkusu Kyokai Gakujutsu Ronbunshi/J. Ceram. Soc. Japan 122 (2014) 393–397, http://dx.doi.org/10.2109/jcersj2.122.393.
[176] M. Nolan, Surface modification of TiO_2 with metal oxide nanoclusters: a route to composite photocatalytic materials, Chem. Commun. 47 (2011) 8617, http://dx.doi.org/10.1039/c1cc13243a.
[177] H. Tong, N. Umezawa, J. Ye, Visible light photoactivity from a bonding assembly of titanium oxide nanocrystals, Chem. Commun. 47 (2011) 4219, http://dx.doi.org/10.1039/c0cc05699e.
[178] S.J. Tauster, Strong metal–support interactions, Acc. Chem. Res. 20 (1987) 389–394, http://dx.doi.org/10.1021/ar00143a001.
[179] M.K.S. Barr, L. Assaud, N. Brazeau, M. Hanbücken, S. Ntais, L. Santinacci, E.A. Baranova, Enhancement of Pd catalytic activity toward ethanol electrooxidation by atomic layer deposition of SnO_2 onto TiO_2 nanotubes, J. Phys. Chem. C 121 (2017) 17727–17736, http://dx.doi.org/10.1021/acs.jpcc.7b05799.
[180] H. Liu, C. Song, L. Zhang, J. Zhang, H. Wang, D.P. Wilkinson, A review of anode catalysis in the direct methanol fuel cell, J. Power Sources 155 (2006) 95–110, http://dx.doi.org/10.1016/j.jpowsour.2006.01.030.
[181] R. Zazpe, J. Prikryl, V. Gärtnerova, K. Nechvilova, L. Benes, L. Strizik, A. Jäger, M. Bosund, H. Sopha, J.M. Macak, Atomic layer deposition Al_2O_3 coatings significantly improve thermal, chemical, and mechanical stability of anodic TiO_2 nanotube layers, Langmuir 33 (2017) 3208–3216, http://dx.doi.org/10.1021/acs.langmuir.7b00187.
[182] M.M. Arafat, B. Dinan, S.A. Akbar, A.S.M.A. Haseeb, Gas sensors based on one dimensional nanostructured metal-oxides: a review, Sensors (Switzerland) 12 (2012) 7207–7258, http://dx.doi.org/10.3390/s120607207.
[183] O.K. Varghese, D. Gong, M. Paulose, K.G. Ong, C.A. Grimes, Hydrogen sensing using titania nanotubes, Sens. Actuators B: Chem. 93 (2003) 338–344, http://dx.doi.org/10.1016/S0925-4005(03)00222-3.
[184] C. Marichy, N. Pinna, Atomic layer deposition to materials for gas sensing applications, Adv. Mater. Interfaces 3 (2016), http://dx.doi.org/10.1002/admi.201600335.
[185] S. Ng, P. Kuberský, M. Krbal, J. Prikryl, V. Gärtnerová, D. Moravcová, H. Sopha, R. Zazpe, F.K. Yam, A. Jäger, L. Hromádko, L. Beneš, A. Hamáček, J.M. Macak, ZnO coated anodic 1D TiO_2 nanotube layers: efficient photo-electrochemical and gas sensing heterojunction, Adv. Eng. Mater. 20 (2018) 1700589, http://dx.doi.org/10.1002/adem.201700589.
[186] J. Bao, I. Shalish, Z. Su, R. Gurwitz, F. Capasso, X. Wang, Z. Ren, Photoinduced oxygen release and persistent photoconductivity in ZnO nanowires, Nanoscale Res. Lett. 6 (2011) 1–7, http://dx.doi.org/10.1186/1556-276X-6-404.
[187] C.C. Li, Z.F. Du, L.M. Li, H.C. Yu, Q. Wan, T.H. Wang, Surface-depletion controlled gas sensing of ZnO nanorods grown at room temperature, Appl. Phys. Lett. 91 (2007) 032101, http://dx.doi.org/10.1063/1.2752541.
[188] C. Liu, E.I. Gillette, X. Chen, A.J. Pearse, A.C. Kozen, M.A. Schroeder, K.E. Gregorczyk, S.B. Lee, G.W. Rubloff, An all-in-one nanopore battery array, Nat. Nanotechnol. 9 (2014) 1031–1039, http://dx.doi.org/10.1038/nnano.2014247.
[189] F. Bonino, L. Busani, M. Lazzari, M. Manstretta, B. Rivolta, B. Scrosati, Anatase as a cathode material in lithium—organic electrolyte rechargeable batteries, J. Power Sources 6 (1981) 261–270, http://dx.doi.org/10.1016/0378-7753(81)80031-6.
[190] S.Y. Huang, L. Kavan, I. Exnar, M. Grätzel, Rocking chair lithium battery based on nanocrystalline TiO_2 (anatase), J. Electrochem. Soc. 142 (1995) L142, http://dx.doi.org/10.1149/1.2048726.
[191] L. Kavan, M. Grätzel, J. Rathouský, A. Zukal, Nanocrystalline TiO_2 (anatase) electrodes: surface morphology, adsorption, and electrochemical properties, J. Electrochem. Soc. 143 (1996) 394, http://dx.doi.org/10.1149/1.1836455.
[192] T. Djenizian, I. Hanzu, P. Knauth, Nanostructured negative electrodes based on titania for Li-ion microbatteries, J. Mater. Chem. 21 (2011) 9925, http://dx.doi.org/10.1039/c0jm04205f.
[193] P.G. Bruce, B. Scrosati, J.-M. Tarascon, Nanomaterials for rechargeable lithium batteries, Angew. Chem. Int. Ed. 47 (2008) 2930–2946, http://dx.doi.org/10.1002/anie.200702505.
[194] G.F. Ortiz, I. Hanzu, T. Djenizian, P. Lavela, J.L. Tirado, P. Knauth, Alternative Li-ion battery electrode based on self-organized titania nanotubes, Chem. Mater. 21 (2009) 63–67, http://dx.doi.org/10.1021/cm801670u.
[195] N.A. Kyeremateng, Self-organised TiO_2 nanotubes for 2D or 3D Li-ion microbatteries, ChemElectroChem 1 (2014) 1442–1466, http://dx.doi.org/10.1002/celc.201402109.
[196] J.B. Goodenough, Y. Kim, Challenges for rechargeable Li batteries, Chem. Mater. 22 (2010) 587–603, http://dx.doi.org/10.1021/cm901452z.
[197] K. Leung, Y. Qi, K.R. Zavadil, Y.S. Jung, A.C. Dillon, A.S. Cavanagh, S.-H. Lee, S.M. George, Using atomic layer deposition to hinder solvent decomposition in lithium ion batteries: first-principles modeling and experimental studies, J. Am. Chem. Soc. 133 (2011) 14741–14754, http://dx.doi.org/10.1021/ja205119g.
[198] T. Dobbelaere, F. Mattelaer, J. Dendooven, P. Vereecken, C. Detavernier, Plasma-enhanced atomic layer deposition of iron phosphate as a positive electrode for 3D lithium-ion microbatteries, Chem. Mater. 28 (2016) 3435–3445, http://dx.doi.org/10.1021/acs.chemmater.6b00853.

[199] M. Kurttepeli, S. Deng, F. Mattelaer, D.J. Cott, P. Vereecken, J. Dendooven, C. Detavernier, S. Bals, Heterogeneous TiO_2/V_2O_5/carbon nanotube electrodes for lithium-ion batteries, ACS Appl. Mater. Interfaces 9 (2017) 8055–8064, http://dx.doi.org/10.1021/acsami.6b12759.
[200] R. Li, Z. Xie, H. Lu, D.W. Zhang, A. Yu, Fabrication of ZnO@TiO_2 core–shell nanotube arrays as three-dimensional anode material for lithium ion batteries, Int. J. Electrochem. Sci. 8 (2013) 11118–11124 http://www.electrochemsci.org/papers/vol8/80911118.pdf.
[201] H. Sopha, G.D. Salian, R. Zazpe, J. Prikryl, L. Hromadko, T. Djenizian, J.M. Macak, ALD Al_2O_3-coated TiO_2 nanotube layers as anodes for lithium-ion batteries, ACS Omega 2 (2017) 2749–2756, http://dx.doi.org/10.1021/acsomega.7b00463.